Master Thesis

Faculty of Electrical Engineering, Mathematics and Computer Science (EEMCS)

Theoretical treatment of streaming potential energy conversion using viscoelastic fluids

Luuk van der Velde, BSc

Examination Committee

Prof. Dr. Jan C.T. Eijkel

Prof. Dr. Devaraj van der Meer

Dr. Ir. Wouter Olthuis

Dr. Ir. Mathieu Odijk

Trieu Nguyen, MSc

2013-5

11th July 2013

BIOS Lab on a Chip group

UNIVERSITY OF TWENTE.

Abstract

During this seven month project the work of Aditya Bandopadhyay and Suman Chakraborty on streaming potentials in viscoelastic fluids is investigated. In their work it is suggested that if the viscoelastic properties match with the electrical an theoretical conversion efficiency of 98.97% is possible.

The theory of streaming potential and viscoelasticity is treated extensively in this report and remarks are given to points which are disputable. Also the mathematical description of the system is simplified and complex integrals are linearised and solved. One major change in the theory is the definition of the input power which is used to calculate the conversion efficiency. Also an external load is added to the system in order to give predictions on how well the system would work as an energy supply.

The change of the definition of the input power results in a theoretical conversion efficiency of 31% and the conversion efficiency at the load will be maximum 22% at 80 kHz using the proposed system of Bandopadhyay.

Preface

Tijdens mijn studie heb ik eigenlijk nooit gedacht aan afstuderen, wanneer ik om mij heen keek naar mensen die aan het afstuderen waren zag ik voornamelijk mensen die het niet leuk vonden. Misschien was ik er wel een beetje bang voor.

Al die onrust was voor niets, ik heb mijn afstudeeronderzoek ervaren als een van de leukste projecten die ik heb gedaan tijdens mijn studie en dat kwam niet alleen door het onderwerp. Ik ben blij dat ik ergens half november bij Jan Eijkel ben binnengelopen voor een 'leuke en uitdagende opdracht,' dat is gelukt. Maar niet zonder de hulp van Jan zelf en Trieu die, als ik als een gek rondjes aan het redeneren was, mij weer op het juiste spoor zetten en weer inspiratie gaven om door te gaan als ik het eventjes niet meer zag zitten.

Inge, ook jou wil ik graag bedanken voor je geduld en je liefde als ik weer moe thuis kwam. Derk, Mathijs, Jan-Yme bedankt voor de afleiding en ondersteuning als ik weer in de knoop zat, omdat ik altijd alles tegelijk wil begrijpen. Verder wil ik Mathijn en Roy bedanken voor hun tijd voor het bedenken hoe ik mijn opstelling zou moeten vullen die Hans zo zorgvuldig in elkaar gezet heeft. Ook wil ik Devaraj, Mathieu en Wouter bedanken dat zij mijn verslag willen beoordelen. Ook de rest van de BIOS groep wil ik bedanken voor de goede verhalen tijdens de lunch en de overvloed aan taart tijdens de koffie en natuurlijk mijn ouders voor de ondersteuning tijdens de afgelopen zeven jaar.

Contents

1 Introduction

At the beginning of the $20th$ century, the existence of a streaming potentials was already known [1]. Streaming potentials and currents are created by a flow of a liquid carrying charges at the solid-liquid interface. Nowadays research is being done for various applications of this electrokinetic phenomenon. It is suggested that, for example, earthquakes can be predicted by measuring streaming potential in the earth's crust [2, 3, 4], seismoelectrictricity is also used for the characterization of oil wells [5]. Streaming current is suggested in micro-/ nanochannels as an energy conversion mechanism as well, both constant pressure [6, 7] and pulsating pressure [8, 9] methods are proposed.

The purpose of this project is to verify a in 2012 by Bandopadhyay and Chakraborty proposed method of *streaming energy* in combination with *viscoelastic fluids* and a *sinusoidal pressure gradient* [10]. The main difference between their work and my work is the point of view. Their research is based on a theoretical point of view, whereas this work takes the practical approach and searches for the boundaries of this phenomenon.

Through first explaining electrodynamics and fluid properties, the extra value of combining the three main concepts (Streaming energy, viscoelastic fluids and the alternating pressure gradient) will become clear at the end of this chapter.

1.1 Electrodynamics

At the interface of a solid and a liquid, the solid will get a surface charge due to interfacial reactions with the liquid (e.g. the dissociation of H^+ molecules in water at a glass surface ($SiOH \rightleftarrows SiO^- + H^+$)[11], which will be assumed throughout this introduction). The channel wall will become negatively charged and, because of conservation of charge, the liquid near the interface becomes slightly positive. This is depicted in the transition from figure 1.1.1a to figure 1.1.1b, where the layer of negative charge at the wall interface is called the 'Surface charge'. Because of electrostatic forces, the surplus of positively charged ions will be attracted to the channel wall, so the bulk becomes neutral. The layer of charges adhered to the wall is called the 'Stern layer.' Because of the screening of the wall by the positive ions and thermal fluctuations (diffusion), not all surplus positive ions are in the Stern layer. This intricate play of attractive and repelling forces results in the so-called 'electrical double layer,' or EDL in short [1, 12, 13] and is schematically shown in 1.1.1c. The thickness of the electrical double layer is characterized by the so called 'Debye length (λ [m]),' named after the Dutch physicist and physical chemist Peter Debye and is in

general in the order of nanometers.

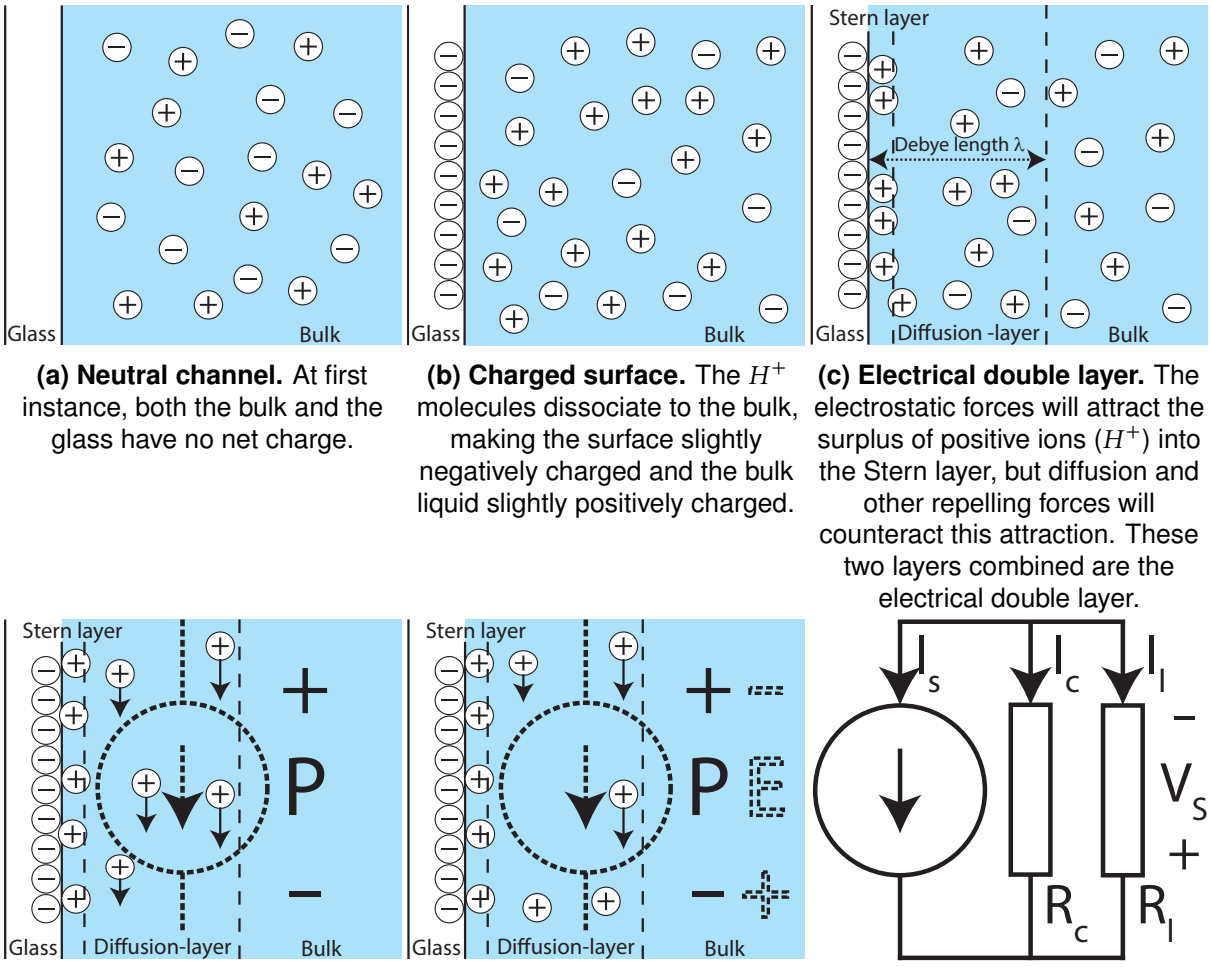

(a) Neutral channel. At first instance, both the bulk and the glass have no net charge.

(b) Charged surface. The H^+ molecules dissociate to the bulk, making the surface slightly negatively charged and the bulk liquid slightly positively charged.

(c) Electrical double layer. The electrostatic forces will attract the surplus of positive ions (H^+) into the Stern layer, but diffusion and other repelling forces will counteract this attraction. These two layers combined are the electrical double layer.

(d) Streaming current. *For simplicity, only the net charge is depicted in this figure.* If an external pressure (P) is applied over the channel, the liquid will start to flow and transport a net flow of positive ions: the streaming current (I_s).

(e) Streaming potential and conduction current. The ion flow will result in a charge gradient over the channel length, creating an electric field (E_s): the streaming potential. Which in turn causes a current in the opposite direction: the conduction current (I_c).

(f) Electrical model Streaming potential modelled as an electrical circuit, with current source I_s, voltage V_s, conduction current and resistance I_c and R_c and load current and resistance I_l and R_l

Figure 1.1.1: A schematical explanation of the streaming potential energy conversion phenomenon.

If an external pressure is applied along the channel, the positive and negative ions in the liquid will follow the flow, but the extra positive ions in the stern layer and the negative ions at the interface remain static. The surplus of positive ions in the double layer will cause a net charge transport, which is also known as an electrical current (streaming current (I_s)), see figure 1.1.1d. Also, if an excess of positive ions flows in one direction they will accumulate at one end and induce a potential difference, or, in other words, a voltage (streaming potential (V_s), figure 1.1.1e)[14]. The streaming current and potential can be used to power a sensor, light or any other device (R_l, figure 1.1.1f).

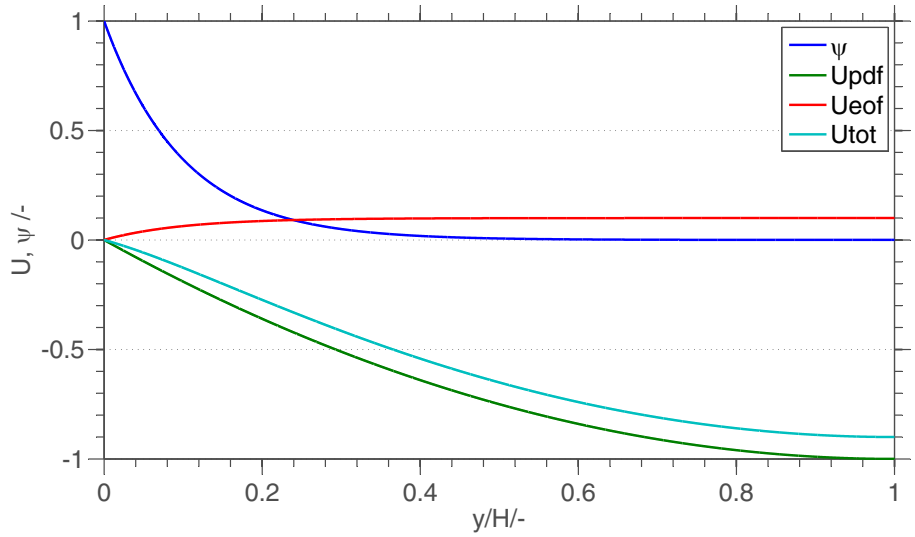

Figure 1.1.2: An overstated example of the electro viscous effect, with the excess of ions in the electrical double layer ψ, the pressure driven flow U_{pdf}, the electro osmotic flow U_{eof} and the resulting flow U_{tot}[15].

However, several secondary effects lower the efficiency of this system, the two main problems are: the conduction current and the finite thickness of the double layer. Since a streaming potential is present over the length of the channel, the ions in the liquid will move due to the electrical forces causes by the streaming potential. This movement of ions results in a current in the opposite direction of the streaming current and is called the conduction current (I_c). This effect can also be modelled in the system by means of a current trough a resistor (R_c), as is depicted in figure 1.1.1f.

Also, the fluid at the centre of the channel does not contribute to the net charge displacement which means that this displacement energy is lost. The loss is even worsened since the centre of the channel does conduct current and hence increases the conduction current and subsequently the conduction current loss.

A third, secondary, problem is called the electro viscous effect. This effect is comparable to an electro osmotic flow, or EOF, and depicted in figure 1.1.2. A pressure applied from top to bottom will result in a pressure driven flow (U_{pdf}), which will induce a streaming potential. Due to this streaming potential, the surplus of charges in the double layer (ψ) will start to move in opposite direction of the applied pressure. Viscous friction will drag along other molecules, resulting in an electro osmotic flow (U_{eof}). The effective flow U_{tot} will therefore be lower than the flow if no streaming potential was present.

Various options are investigated in order to overcome these losses. One solution is to increase the surface/ volume ratio. This can be achieved by decreasing the channel width and/ or height (e.g. nano-channels). A higher surface/ volume ratio results in a higher ratio of contributing fluid transport over useless fluid transport [6, 7]. However, the increase of surface/ volume ratio results in a higher

surface friction and thus higher friction loss (a maximum theoretical conversion efficiency of 15% in no slip conditions, up to 30% if slip is allowed[16]). In order to decrease this surface friction, researchers proposed to modifying the surface with large ions to increase the slip length, resulting in a maximum theoretical conversion efficiency of $> 50\%$[16]. A downside of this approach is that it is a quite intricate procedure to accomplish this.

Recently, a theoretical paper claimed that it is possible to get an conversion efficiency of almost $100\,\%$ if viscoelastic fluids are used inside nano-channels using an alternating pressure gradient [10]. This theory will be used throughout this thesis and experiments will be developed to investigate the claims.

1.2 Fluid dynamics

Normally in fluid dynamics, it is assumed that liquids behave Newtonian, that is that the viscosity is constant in any circumstance. Viscosity is the proportionality factor between sheer rate and sheer stress, defined through the equation $F = \eta A(dv/dx)$, where F is the tangential force required to move a planar surface of area A at velocity v relative to a parallel surface separated from the first by a distance x[17]. In other words: it is, for example, hard to move a spoon through a cup of honey (which has relative high viscosity), compared to move the same spoon through a cup of water (with relative low viscosity). Therefore the flow in a microchannel of a liquid having high viscosity will be lower than the flow of a low viscosity liquid.

However, Non-Newtonian fluids exists as well, these fluids have a viscosity depending on for example the shear rate. In that case they are called viscoelastic. Multiple viscoelastic liquids exist, commonly known viscoelastic liquids are polymer melts and crude oil.

Lots of cosmetic products (e.g. shampoo and hair gel) are viscoelastic as well, these properties are caused by micelles, which will also be used during the experiments. Micelles are generally clustered groups of amphiphilic ('loves both') molecules: molecules which have a hydrophilic ('water-loving') head group and lipophilic ('fat-loving') tail. When these molecules are passed into water the tails will cluster together, forming either spherical, lamellar (flat) or wormlike (tube) micelles. If the concentration of additive is increased, the micelles will form interconnections and form a highly viscous gel, see figure 1.2.1. At the transition from wormlike to interconnected micelles the fluid behaves like a polymer melt, but its 'polymers' can break-up and combine and are therefore called 'living polymers'.

A model which describes the mechanical behaviour of the micelle solution for low frequencies is the Maxwell model [19, 20], which consists of a spring and a dashpot (as is depicted in figure 1.2.2). In figure 1.2.3 the response of a viscoelastic material is shown. If a strain is applied, the material will have a high stress and relax gradually. The frequency response of a Maxwell material is shown in figure 1.2.4

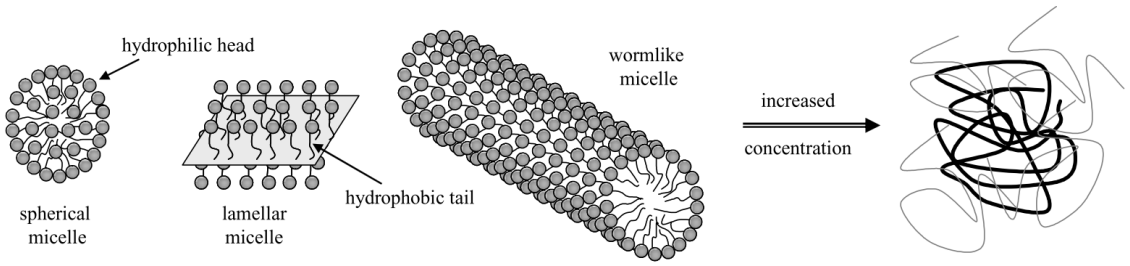

Figure 1.2.1: Three different kinds of micelles: spherical, lamellar and wormlike. With an high concentration, the wormlike micelles entangle and behave like 'living polymers'. From: [18]

Figure 1.2.2: The Maxwell model can be represented by a purely viscous damper and a purely elastic spring connected in series, picture from: Wikipedia.

it can be seen that at higher frequencies, the material becomes less viscous and more and more elastic. Also, the loss increases in the beginning, but gradually becomes less. According to Bandopadhyay and Chakraborty [10], the use of Maxwell fluids will greatly increase the energy conversion from the hydraulic domain to the electric domain.

1.3 Research goals

The goals of this project are 1) to understand the mechanism behind the giant augmentations of the streaming energy; 2) to model physics causing the streaming energy; 3) to design an experiment with which the claimed augmentations can be investigated; 4) to build an experimental set up to measure the mechanical input and electrical output power; and 5) to perform the experiments.

To achieve this, the theory of Bandopadhyay and Chakraborty [10, 21] is first analysed in chapter 2 and discussed in chapter 3. In chapter 4 a method is proposed to measure the output energy. Which is followed by the results of the theoretical work in chapter 5, since no measurements are conducted. The conclusions derived from the results are presented in chapter 6. A list of used abbreviations, definitions and symbols can be found in appendix A.

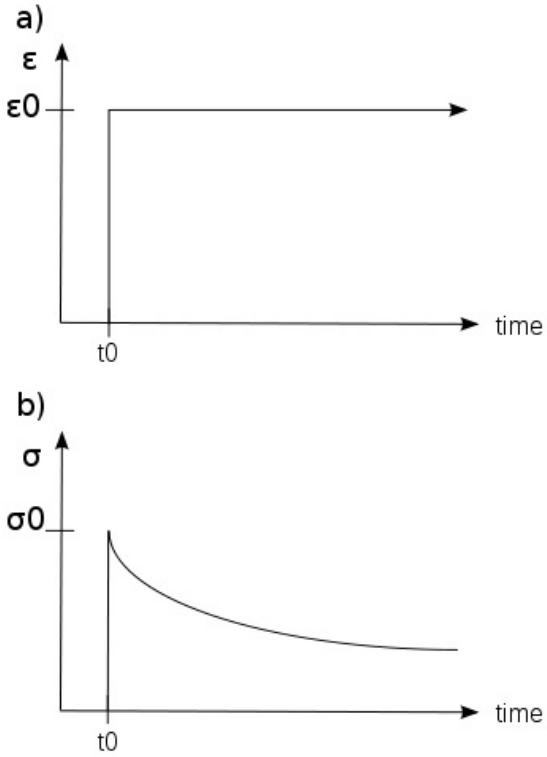

Figure 1.2.3: a) Applied strain and b) induced stress as functions of time for a viscoelastic material, picture from: Wikipedia.

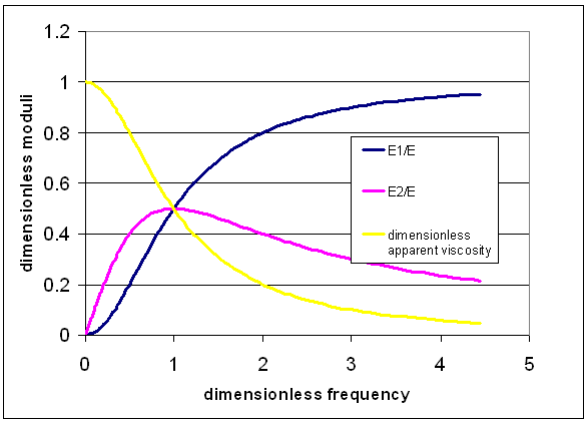

Figure 1.2.4: Relaxational spectrum for Maxwell material, picture from: Wikipedia.

2 Bandopadhyay's and Chakraborty's theoretical work

The first part of this chapter will be about the work Bandopadhyay and Chakraborty did, but in a less confined matter than their paper [10], with some more details found in an preceding paper [21].

2.1 Electrical double layer

The electrical double layer (schematically shown in figure 2.1.2) can can also be expressed in a mathematical form, using the Poisson equation (2.1.1) as a starting point:

$$\nabla^2\psi(y) = -\rho_e(y)/\epsilon \ [\mathrm{V/m^2}] \tag{2.1.1}$$

where y [m] is the coordinate direction normal to the confining boundaries (distance from the wall), ψ [V] the potential distribution, ρ_e is the charge density distribution and ϵ [F/m] the dielectric constant of the medium.

The charge density distribution is given by:

$$\rho_e(y) = e(z^+n^+(y) + z^-n^-(y)) \ [\mathrm{C/m^3}] \tag{2.1.2}$$

in which e [C] is the elementary charge, $z^\pm$ [–] and $n^\pm$ [1/m^3] are the valence and the ionic number densities of the charge species respectively. If the EDL is non-overlapping, the ionic advection from wall to wall is negligible compared to the ionic diffusion and the ions are idealized as point charges, the ionic number densities are expressed by the Boltzmann distribution:

$$n_\pm(y) = n_\mathrm{o}e^{-z^\pm e\psi(y)/k_BT} \ [\mathrm{1/m^3}] \tag{2.1.3}$$

where n_o [1/m^3] is the bulk ionic concentration, k_B [J/K] Boltzmann's constant and T [K] the temperature. If (2.1.2) and (2.1.3) are substituted in (2.1.1) and a $z:z$ electrolyte is assumed, this leads to:

$$\frac{d^2\psi(y)}{dy^2} = \frac{2zen_\mathrm{o}}{\epsilon}\sinh\left(\frac{ze\psi(y)}{k_BT}\right) \ [\mathrm{V/m^2}] \tag{2.1.4}$$

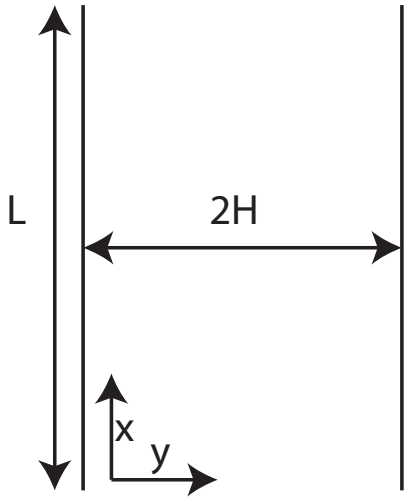

Figure 2.1.1: The definitions of the channel

Or, in dimensionless form:

$$\frac{d^2\bar{\psi}(\bar{y})}{d\bar{y}^2} = \frac{1}{\bar{\lambda}^2\bar{\zeta}}\sinh(\bar{\zeta}\bar{\psi}(\bar{y}))\ [-] \tag{2.1.5}$$

with dimensionless parameters $\bar{\psi}(\bar{y}) = \psi(y)/\zeta$ [–] (with ζ [V] the ζ-potential, being the electric potential at the surface relative to the potential in the bulk medium at a long distance and is also called electrokinetic potential [17]), $\bar{\zeta} = ze\zeta/k_BT$ [–], $\bar{y} = y/H$ [–] (H [m] being the half-height of the channel) and $\bar{\lambda} = \lambda/H$ [–], λ [m] being the Debye length (a measure for the length scale of the EDL), defined as $\lambda = \sqrt{\epsilon k_BT/2z^2e^2n_0}$ [m] $= 0.304/\sqrt{I(M)}$ [nm], with I the ionic strength in molar (mol/L). If (2.1.5) is subjected to the following boundary conditions: at $\bar{y} = 0 \Rightarrow \bar{\psi}(\bar{y}) = 1$ and at $\bar{y} = 1 \Rightarrow d\bar{\psi}(\bar{y})/d\bar{y} = 0$ the EDL potential is described as:

$$\bar{\psi}(\bar{y}) = \frac{4}{\bar{\zeta}}\operatorname{atanh}\left(\tanh\left(\frac{\bar{\zeta}}{4}\right)e^{-\bar{y}/\bar{\lambda}}\right) \text{ for } 0 \le \bar{y} \le 1\ [-] \tag{2.1.6}$$

Throughout the report the boundary condition $0 \le \bar{y} \le 1$ will be taken into account. If the zeta potential is sufficently low ($|\zeta| < 25$ mV, $|\bar{\zeta}| < 1$), (2.1.6) can be simplified into:

$$\bar{\psi}(\bar{y}) = \frac{\cosh\left((1-\bar{y})/\bar{\lambda}\right)}{\cosh\left(1/\bar{\lambda}\right)}\ [-] \tag{2.1.7}$$

Another simplification can be done, which will be discussed in section 3.1.1.

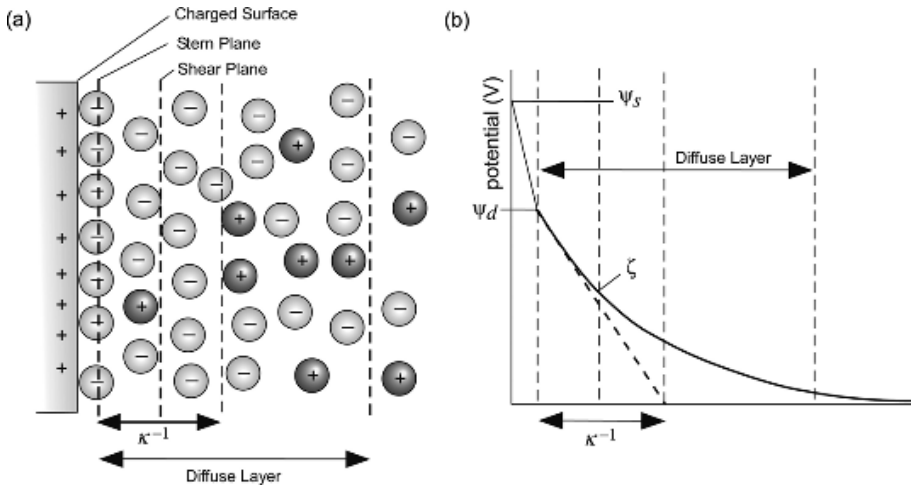

Figure 2.1.2: (a) Physical picture of the Stern model of the electrical double layer, with κ^{-1} the Debye length. (b) One of the possible potential distributions of the Stern model, the potential at the shear plane is called the 'ζ(zeta) -potential'. This model assumes that in the Stern layer the potential varies linearly. [22]

2.2 Flow profile

Having the electrical double layer represented mathematically, the fluid behaviour can be described. Fluid dynamics is based on the Navier-Stokes equation[22]:

$$\rho\left(\frac{\partial \boldsymbol{v}}{\partial t} + \boldsymbol{v}\cdot\nabla\boldsymbol{v}\right) = -\nabla p + \nabla\cdot\boldsymbol{T} + \rho\boldsymbol{g} + \boldsymbol{f}\ [\mathrm{N/m^3}] \tag{2.2.1}$$

where ρ [kg/m^3] is the fluid density, $\boldsymbol{v}$ [m/s] is the velocity vector, p [Pa] the pressure, $\boldsymbol{T}$ [N/m^2] the stress tensor, $\boldsymbol{g}$ the gravitational forces and $\boldsymbol{f}$ [N/m^3] are the other body forces. Since the fluid is assumed to be incompressible $\nabla\boldsymbol{v} = 0$ [/s] $\Rightarrow \boldsymbol{v}\cdot\nabla\boldsymbol{v} = 0$ [m/s^2], the stress in the channel is only caused by the viscous stress, so $\boldsymbol{T} = \boldsymbol{\tau}$ ($\boldsymbol{\tau}$ being the stress tensor). Gravitational forces are negligible in microchannels and the other body forces are generated only by the induced electric potential (which is explained in section 2.3.1) and the net ionic charge density (ρ_e): $\boldsymbol{f} = \rho_e(y)\boldsymbol{E}$. Using these details, (2.2.1) becomes:

$$\rho\frac{\partial \boldsymbol{v}}{\partial t} = -\nabla p + \nabla\cdot\boldsymbol{\tau} + \rho_e\boldsymbol{E}\ [\mathrm{N/m^3}] \tag{2.2.2}$$

$\boldsymbol{\tau}$ is modelled as a linearised Maxwell fluid which is reliable for low Reynolds numbers ($Re < 1\times10^{-3}$, which is explained in section 3.3) and low (0.60/s) shear rates [23]. The stress tensor of a linearised Maxwell fluid is modelled as[24]

$$\boldsymbol{\tau} = \eta\nabla\boldsymbol{v} - t_m\frac{\partial\boldsymbol{\tau}}{\partial t}\ [\mathrm{N/m^2}] \tag{2.2.3}$$

Where η [Pa s] is the viscosity and t_m [s] the relaxation time of the liquid, these two parameters characterize the linearised Maxwell fluid. The velocity and pressure only changes in x-direction, so the velocity profile is:

$$\boldsymbol{v} =< v_x(y,t), \mathrm{o}, \mathrm{o} >= v_x(y,t) = u(y,t) \text{ [m/s]} \tag{2.2.4}$$

and the pressure gradient becomes:

$$\nabla p(x(t), y(t), z(t)) = \frac{\partial p(x,t)}{\partial x} \text{ [Pa/m]} \tag{2.2.5}$$

The electric field $\boldsymbol{E}$ exists only in x-direction, therefore:

$$\boldsymbol{E} =< E_x(t), \mathrm{o}, \mathrm{o} >= E_x(t) = E_s(t) \text{ [V/m]} \tag{2.2.6}$$

The change in stress (i.e. $\nabla \frac{\partial \boldsymbol{\tau}}{\partial t}$ [N/(m^3 s)]) is caused by three phenomena: the acceleration of the flow ($\rho \frac{\partial^2 u(y,t)}{\partial t^2}$ [N/(m^3 s)]), the change in pressure over time and x ($\frac{\partial}{\partial t}\frac{\partial p(x,t)}{\partial x}$ [N/(m^3 s)]) as well as the change of E_s over time ($-\rho_e(y)\frac{dE_s(t)}{dt}$ [N/(m^3 s)]). If these assumptions are inserted into (2.2.3) and then into (2.2.2), it becomes:

$$\begin{aligned}
\rho \frac{\partial u(y,t)}{\partial t} &= -\frac{\partial p(x,t)}{\partial x} + \nabla \cdot \left(\eta \nabla u(y,t) - t_m \frac{\partial \boldsymbol{\tau}}{\partial t} \right) + \rho_e(y) E_s(t) \\
&= -\frac{\partial p(x,t)}{\partial x} + \eta \nabla^2 u(y,t) - t_m \nabla \frac{\partial \boldsymbol{\tau}}{\partial t} + \rho_e(y) E_s(t) \\
&= -\frac{\partial p(x,t)}{\partial x} + \eta \nabla^2 u(y,t) - t_m \left(\rho \frac{\partial^2 u(y,t)}{\partial t^2} + \frac{\partial}{\partial t}\frac{\partial p(x,t)}{\partial x} - \rho_e(y)\frac{dE_s(t)}{dt} \right) \\
&\quad + \rho_e(y) E_s(t) \text{ [N/m}^3\text{]}
\end{aligned} \tag{2.2.7}$$

$u(y,t)$ [m/s] only changes in the y direction, thus $\nabla^2 u(y,t) = \frac{\partial^2 u(y,t)}{\partial y^2}$ [1/(s m)]. $\psi(y)$ [V] changes only in y direction also, so (2.1.1) becomes $\rho_e(y) = -\epsilon \frac{d^2\psi(y)}{dy^2}$ [C/m^3]. Both are inserted into (2.2.7), all terms with $u(y,t)$ [m/s] are shifted to the left hand side of the equation and the equation is devided by η [Pa s], which results in:

$$\begin{aligned}
&\frac{\partial^2 u(y,t)}{\partial y^2} - \frac{\rho}{\eta}\left(\frac{\partial u(y,t)}{\partial t} + t_m \frac{\partial^2 u(y,t)}{\partial t^2} \right) = \\
&\frac{1}{\eta}\frac{\partial p(x,t)}{\partial x}\left(1 + t_m \frac{\partial}{\partial t} \right) + \frac{\epsilon}{\eta}\frac{d^2\psi(y)}{dy^2}\left(E_s(t) + t_m \frac{dE_s(t)}{dt} \right) \text{ [1/(m s)]}
\end{aligned} \tag{2.2.8}$$

Then the Fourier transform of this equation is taken and $\omega = -\omega$:

$$\begin{aligned}&\frac{\partial^2 U(y,\omega)}{\partial y^2} + U(y,\omega)\frac{\rho}{\eta}\left(i\omega + t_m\omega^2\right) = \\ &\frac{1}{\eta}\frac{\partial P(x,\omega)}{\partial x}(1 - i\omega t_m) + \frac{\epsilon\tilde{E}_s(\omega)}{\eta}\frac{d^2\psi(y)}{dy^2}(1 - i\omega t_m)\ [1/(\mathrm{m\,s})]\end{aligned} \tag{2.2.9}$$

Where $U(y,\omega) = \mathcal{F}\{u(y,t)\}$, $P(x,\omega) = \mathcal{F}\{p(x,t)\}$ and $\tilde{E}_s(\omega) = \mathcal{F}\{E_s(t)\}$. This equation is made non-dimensional using the following normalizations: $U^*(\bar{y},\omega) = \frac{U(\bar{y}H,\omega)\eta}{\frac{\partial P(x,\omega)}{\partial x}H^2}$ [−], $\bar{E}_s(\omega) = \frac{\tilde{E}_s(\omega)\epsilon\zeta}{\frac{\partial P(x,\omega)}{\partial x}H^2}$ [−], $\omega^* = \omega t_m$ [−], $\bar{\omega} = i\omega^* + \omega^{*2}$ [−], $\beta^2 = \frac{\rho(\omega^{*2} + i\omega^*)}{\eta t_m}$ [1/m^2] and $\frac{\partial^2\bar{\psi}}{\partial\bar{y}^2}$ [−] is given by (2.1.5). Therefore (2.2.9) becomes:

$$\frac{\partial^2 U^*(\bar{y},\omega)}{\partial\bar{y}^2} + U^*(\bar{y},\omega)\beta^2 H^2 = (1 - i\omega^*) + \bar{E}_s(\omega)\frac{\sinh(\bar{\psi}\bar{\zeta})}{\bar{\lambda}^2\bar{\zeta}}(1 - i\omega^*)\ [-] \tag{2.2.10}$$

Where $\beta^2 H^2/\bar{\omega} = \frac{\rho H^2}{\eta t_m}$ is defined as α, which is the inverse of the dimensionless Deborah number (De), indicating how viscoelastic a material behaves [25] . Using the two standard boundary conditions: zero flow at the wall interface ($\bar{y} = 0 \Rightarrow U^* = 0$) and symmetry ($\bar{y} = 1 \Rightarrow \frac{\partial U^*}{\partial\bar{y}} = 0$) U^* can be solved to:

$$\begin{aligned}U^*(\bar{y},\omega) = &\left(\frac{1 - i\omega^*}{\alpha\bar{\omega}}\right)\left(1 - \frac{\cos\left(\sqrt{\alpha\bar{\omega}}(1-\bar{y})\right)}{\cos\left(\sqrt{\alpha\bar{\omega}}\right)}\right) \\ &+ \bar{E}_s(\omega)\frac{1 - i\omega^*}{\bar{\zeta}\bar{\lambda}^2\sqrt{\alpha\bar{\omega}}}\Bigg[-\cos\left(\sqrt{\alpha\bar{\omega}}\bar{y}\right)\int_0^{\bar{y}}\sinh\left(\bar{\psi}(\bar{y})\bar{\zeta}\right)\sin\left(\sqrt{\alpha\bar{\omega}}\bar{y}\right)d\bar{y} \\ &+ \sin\left(\sqrt{\alpha\bar{\omega}}\bar{y}\right)\int_0^{\bar{y}}\sinh\left(\bar{\psi}(\bar{y})\bar{\zeta}\right)\cos\left(\sqrt{\alpha\bar{\omega}}\bar{y}\right)d\bar{y} \\ &+ \sin\left(\sqrt{\alpha\bar{\omega}}\bar{y}\right)\tan\left(\sqrt{\alpha\bar{\omega}}\right)\int_0^{1}\sinh\left(\bar{\psi}(\bar{y})\bar{\zeta}\right)\sin\left(\sqrt{\alpha\bar{\omega}}\bar{y}\right)d\bar{y} \\ &+ \sin\left(\sqrt{\alpha\bar{\omega}}\bar{y}\right)\int_0^{1}\sinh\left(\bar{\psi}(\bar{y})\bar{\zeta}\right)\cos\left(\sqrt{\alpha\bar{\omega}}\bar{y}\right)d\bar{y}\Bigg]\ [-]\end{aligned} \tag{2.2.11}$$

Using the Debye-Hückel linearisation (see section 3.1), this equation can be simplified into:

$$\begin{aligned}U^*(\bar{y},\omega) = &\left(\frac{1 - i\omega^*}{\alpha\bar{\omega}}\right)\left(1 - \frac{\cos\left(\sqrt{\alpha\bar{\omega}}(1-\bar{y})\right)}{\cos\left(\sqrt{\alpha\bar{\omega}}\right)}\right) \\ &+ \bar{E}_s(\omega)\frac{1 - i\omega^*}{1 + \alpha\bar{\omega}\bar{\lambda}^2}\left(\frac{\cosh\left((1-\bar{y})/\bar{\lambda}\right)}{\cosh\left(1/\bar{\lambda}\right)} - \frac{\cos\left(\sqrt{\alpha\bar{\omega}}(1-\bar{y})\right)}{\cos\left(\sqrt{\alpha\bar{\omega}}\right)}\right)\ [-]\end{aligned} \tag{2.2.12}$$

Equation (2.2.12) can be split into two parts, a Poiseuille flow for viscoelastic fluids (first part, $U_p^*(\bar{y},\omega^*)$) which flows because of a pressure difference and a flow (second part, $\bar{E}_s(\omega^*)U_E^*(\bar{y},\omega^*)$) which flows because of an electrical potential (note that $\frac{\cosh((1-\bar{y})/\bar{\lambda})}{\cosh(1/\bar{\lambda})} = \bar{\psi}(\bar{y})$ [V] and refer to figure 1.1.2). This flow results an a higher apparent viscosity and is therefore called the electro-viscous effect. Adding the two results in a more convenient description of the total flow:

$$U^*(\bar{y},\omega^*) = U_p^*(\bar{y},\omega^*) + \bar{E}_s(\omega^*)U_E^*(\bar{y},\omega^*)\ [-] \tag{2.2.13}$$

2.3 Electro-hydro-dynamic energy conversion efficiencies

The conversion efficiency (η_{eff} [−]) is defined as the electrical (output) power ($P_{elec} =< I_c(\omega)E_s(\omega) >_t$ [W/m^3]), with I_c [A/m^2] the conduction current density and E_s [V/m] the streaming potential, over the hydrodynamic (input) power ($P_{hydr} =< \frac{dP(x,\omega)}{dx}Q(\omega) >_t$ [W/m^3]), with $\frac{dP}{dx}$ [Pa/m] the pressure gradient over the length of the channel and Q [m/s] the flow density.

$$\eta_{eff}(\omega) = \frac{P_{elec}}{P_{hydr}} = \frac{< I_c(\omega)E_s(\omega) >_t}{< \frac{dP(x,\omega)}{dx}Q(\omega) >_t}\ [-] \tag{2.3.1}$$

In the following sections, the streaming potential and the other electrical effects will be discussed.

2.3.1 Streaming potential

As a recap from the introduction: if a pressure gradient is applied over the channel, the mobile charge will, due to viscous drag, move with the fluid. This results in a net moving charge and thus a current. Furthermore there will be a charge gradient along the channel imposing a potential over the length of the channel. These two phenomena are called the streaming current and streaming potential respectively.

Since the flow profile is dependent on the streaming potential, which in turn is dependent on the flow profile, equation (2.2.12) must be closed. This is done by using Kirchhoff's law: the sum of all currents is zero, therefore:

$$A(I_s + I_c + I_{Du}) = 0\ [\mathrm{A}] \tag{2.3.2}$$

With A [m^2] the area of the channel cross section, I_s [A/m^2] the streaming current density, I_c [A/m^2] the bulk conduction current density and I_{Du} [A/m^2] the surface conduction current density.

2.3.2 Streaming current density

The net charge contributes to the streaming current, so the streaming current density is defined as the integral over the height of the channel of the concentration difference ($ze(n^+(y) - n^-(y))$ [C/m^3]) times the flow profile ($U(y,\omega)$ [m/s]):

$$I_s(\omega) = \int_0^H ze(n^+(y) - n^-(y))U(y,\omega)dy \text{ [A/m}^2\text{]} \tag{2.3.3}$$

Using the Boltzmann distribution (2.1.3) and the already discussed parameters:

$$n_+(y) - n_-(y) = 2n_0 \sinh\left(\frac{z\psi(y)}{V_T}\right) \text{ [1/m}^3\text{]} \tag{2.3.4}$$

plugging this in (2.3.3) results in:

$$I_s(\omega) = 2zen_0 \int_0^H \sinh\left(\frac{z}{V_T}\psi(y)\right)U(y,\omega)dy \text{ [A/m}^2\text{]} \tag{2.3.5}$$

Where $V_T = k_B T/e \approx 25$mV is the thermal voltage, k_B Boltzmann's constant and T the temperature. (2.3.5) can not be solved analytically and will be made dimensionless in section B.1 for further use.

2.3.3 Bulk conduction current density

The conduction current consists of two parts: the bulk conduction current, which is called conduction current from now on and is caused by the conductivity of the bulk electrolyte. The other part is the surface conduction current (or 'Stern-layer conduction'), which is caused by the conductance along the liquid/wall interface.

For the conduction current the total concentration ($ze(n^+(y) + n^-(y))$ [C/m^3]) contributes and is multiplied by an ionic unit flow $\frac{zeE_s(\omega)}{f}$ [m/s] and integrated to get the current density:

$$I_c(\omega) = \int_0^H \frac{z^2e^2E_s(\omega)}{f}(n^+(y) + n^-(y))dy \text{ [A/m}^2\text{]} \tag{2.3.6}$$

with f [kg/s] the ionic friction coefficient, which cannot be found in literature, but is defined by Bandopadhyay as:

$$f = \frac{2n_0z^2e^2}{\sigma_b} \text{ [kg/s]} \tag{2.3.7}$$

where σ_b [S/m] is the conductivity of the bulk electrolyte and using Boltzmann's distribution:

$$n_+(y) + n_-(y) = 2n_0 \cosh\left(\frac{z\psi(y)}{V_T}\right) \text{ [1/m}^3\text{]} \tag{2.3.8}$$

Ultimately, (2.3.6) becomes:

$$I_c(\omega) = E_s(\omega)\sigma_b \int_0^H \cosh\left(\frac{z}{V_T}\psi(y)\right) dy \text{ [A/m}^2\text{]} \tag{2.3.9}$$

Which will be solved in (3.1.11).

2.3.4 Stern-layer conduction current density

The Stern-layer conduction current density is defined using the Duhkin number, which relates the bulk conductance to the Stern-layer conductance (σ_{st} [S]) as $Du = \frac{\sigma_{st}}{H\sigma_b}$. This gives:

$$I_{Du}(\omega) = E_s(\omega)\sigma_b Du = E_s(\omega)\sigma_{st}/H \text{ [A/m}^2\text{]} \tag{2.3.10}$$

2.3.5 Streaming potential, continued

All currents are known and can be plugged into equation (2.3.2) and is divided by the cross sectional area (A [m^2]), resulting in:

$$2zen_0 \int_0^H \sinh\left(\frac{z}{V_T}\psi(y)\right) U(y,\omega) dy + E_s(\omega)\sigma_b \int_0^H \cosh\left(\frac{z}{V_T}\psi(y)\right) dy + E_s(\omega)\sigma_b Du = 0 \text{ [A/m}^2\text{]} \tag{2.3.11}$$

Using the known normalization parameters and $J = \frac{\sigma_b \eta \lambda^2}{\epsilon^2 \zeta^2}$ [−], equation (2.3.11) is simplified into (see appendix B.1 for more details):

$$\iota_1(\omega^*) + \bar{E}_s \iota_2(\omega^*) + J\iota_3 \bar{E}_s + JDu\bar{E}_s = 0 \text{ [−]} \tag{2.3.12}$$

where $\iota_1(\omega^*) = \int_0^1 U_p^*(\bar{y},\omega^*)\frac{\sinh(\bar{\zeta}\bar{\psi}(\bar{y}))}{\bar{\zeta}} d\bar{y}$, $\iota_2(\omega^*) = \int_0^1 U_E^*(\bar{y},\omega^*)\frac{\sinh(\bar{\zeta}\bar{\psi}(\bar{y}))}{\bar{\zeta}} d\bar{y}$ and $\iota_3 = \int_0^1 \cosh(\bar{\zeta}\bar{\psi}(\bar{y})) d\bar{y}$, to obtain the streaming potential, (2.3.12) is rearranged to:

$$\bar{E}_s(\omega^*) = \frac{-\iota_1(\omega^*)}{\iota_2(\omega^*) + J(\iota_3 + Du)} \text{ [−]} \tag{2.3.13}$$

2.4 Volumetric flow density

Now the last unknown parameter for the conversion efficiency, the volumetric flow density Q [m/s], or flow density, has to be described and it is defined as the integral of the flow profile over the height of the channel:

$$Q(\omega) = \int_0^H U(y,\omega)dy/H \text{ [m/s]} \tag{2.4.1}$$

But, since all parameters are dimensionless, also a dimensionless flow density is defined:

$$Q^*(\omega) = \int_0^1 U^*(\bar{y},\omega)d\bar{y} = \frac{Q(\omega)\eta}{\frac{\partial P(x,\omega)}{\partial x}H^2} \text{ [–]} \tag{2.4.2}$$

This integral will be solved in (3.1.6).

2.5 Conversion efficiency from normalized parameters

The definition of the conversion energy is the electrical output power over the mechanical/ hydraulic input power and is given in: (2.3.1). The conversion efficiency is rewritten into a form with only normalized numbers in (3.1.13):

$$\eta_{eff}(\omega) = \frac{P_{elec}}{P_{hydr}} = \frac{< I_c(\omega)E_s(\omega) >_t}{< \frac{dP(x,\omega)}{dx}Q(\omega) >_t} = \frac{J\bar{E}_s^2(\omega)\iota_3}{Q^*(\omega)\bar{\lambda}^2} \text{ [–]} \tag{2.5.1}$$

all parameters are already described above. This equation is used to plot figure 2.5.1a. The figure is identical to the one Bandopadhyay and Chakraborty produced, so the derivation of the equations is correct. In order to compress the plot even more the normalized frequency (ω^*) is multiplied by $\sqrt{\alpha}$ in figure 2.5.1b to shift all peaks to one point. It can be seen that the conversion efficiency is over98%, which is far more than the efficiencies mentioned in other papers[6, 8, 9, 16]. It must be noted that not al electrical energy can be harvested, since there always will be a loss in the energy transfer.

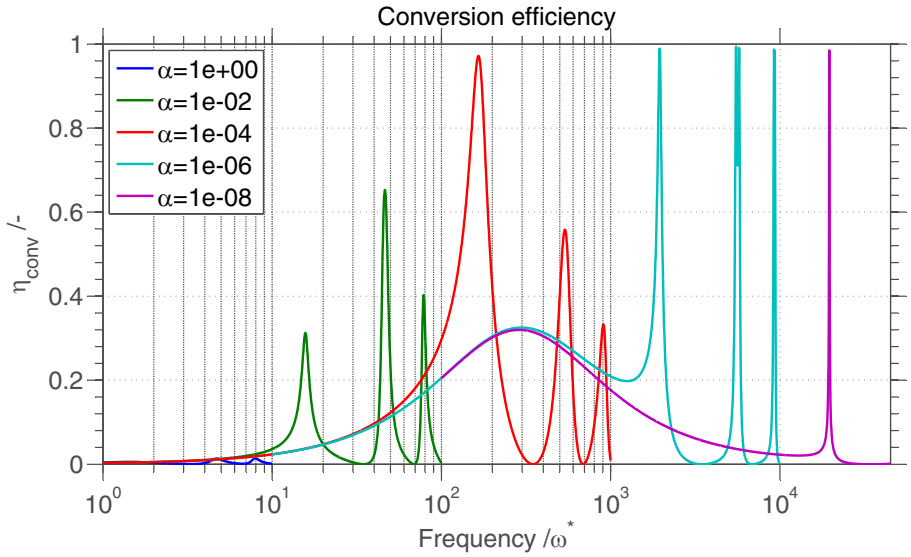

(a) Remake of figure 2b. from Bandopadhyay's paper[10]: η_{conv} vs ω^*, with parameters $\bar{\lambda} = 1/10$, $J = -10$, $\bar{\zeta} = -1$ and varying α

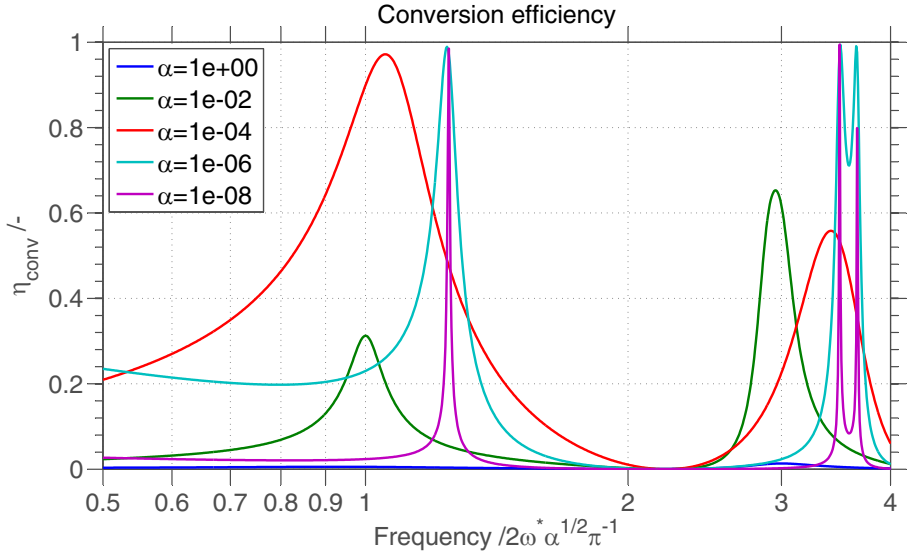

(b) Rescaled remake of figure 2b. from Bandopadhyay's paper[10]: η_{conv} vs $2\omega^*\sqrt{\alpha}/\pi$, with parameters $\bar{\lambda} = 1/10$, $J = -10$, $\bar{\zeta} = -1$ and varying α

Figure 2.5.1: Comparison of the two plot techniques using 3.1.13, in (a) the x-axis is only normalized by the relaxation time. In (b) the x-axis is also normalized by $\sqrt{\alpha}$.

3 My comments on the work of Bandopadhyay and Chakraborty

In this and the following chapters some key discussion points regarding the work done by Bandopadhyay and Chakraborty are discussed. First, the unsolved integrals from Bandopadhyay's theory will be solved by applying the Debye-Hückel linearisation to the double layer potential. Then the relation between the non-dimensinal and dimensional parameters is given. Followed by some remarks on the Reynolds number, the J parameter and the Dukhin number. Next the optimal frequency is estimated and viscoelastic fluids are discussed. This is followed by a discussion what the influence of all parameters is onto the system and it will be shown that most parameters are really entangled and it is hard to make a compromise. In the last three sections a load resistance will be added, the flowprofile is investigated and the efficiency is redefined.

3.1 Integration and linearisation

During the derivation of the model presented by Bandopadhyay and Chakraborty, lots of integrals were presented and not yet solved. Using the linearisation of the electrical double layer they can be solved analytically and simplified drastically. This will be done in this section for first the electrical double layer potential; then the cosine terms in the flow profile are investigated; followed by the determination of the flow density; and finally the integrals of the streaming potential are solved and then simplified even further.

Since the theory presented by Bandopadhyay is only valid with no double layer overlap: $\bar{\lambda} < 1/10$ and the boundary condition of a low ζ-potential $|\zeta| < 25\,\text{mV}$ or $|\bar{\zeta}| < 1$, these assumptions will also be made during this analysis. The terms which become negligible because of these assumptions are marked in red and denoted by a $\diamond$.

3.1.1 Electrical double layer potential

Bandopadhyay and Chakraborty[21] model the double layer potential mathematically by the following relation (2.1.6):

$$\bar{\psi}_1(\bar{y}) = \frac{4}{\bar{\zeta}} \operatorname{atanh}\left(\tanh\left(\frac{\bar{\zeta}}{4}\right) e^{\left(\frac{-\bar{y}}{\bar{\lambda}}\right)}\right) \text{ for } 0 \leq \bar{y} \leq 1 \text{ [–]} \tag{3.1.1}$$

and later they suggest that it if low ζ-potentials ($\zeta < 25\,\text{mV}$) are assumed (3.1.1) can be simplified into (2.1.7):

$$\bar{\psi}_2(\bar{y}) = \frac{\cosh\left((1-\bar{y})/\bar{\lambda}\right)}{\cosh\left(1/\bar{\lambda}\right)} \text{ [–]} \tag{3.1.2}$$

another simpler and widespread used model for the EDL potential is to take a first order Taylor expansion around zero of $\tanh$ and atanh: $\tanh(x) \approx \operatorname{atanh}(x) \approx x + O(x^3)\diamond$, which is accurate enough since $\bar{\zeta}/4 \leq 0.25$ and results in the Debye-Hückel linearization [22]:

$$\bar{\psi}_3(\bar{y}) = e^{-\bar{y}/\bar{\lambda}} \text{ [–]} \tag{3.1.3}$$

Now, the normalized double layer potential can be integrated over the height ($d\bar{y}$) of the channel:

$$\int_0^1 \bar{\psi}_3 d\bar{y} = \int_0^1 e^{-\bar{y}/\bar{\lambda}}\, d\bar{y} = \bar{\lambda}\left(1 - e^{-1/\bar{\lambda}}\diamond\right) \approx \bar{\lambda} \text{ [–]} \tag{3.1.4}$$

Since $1/\bar{\lambda} > 10 \Rightarrow e^{-1/\bar{\lambda}} < 4.5 \times 10^{-5}$, the exponential term will be neglected.

3.1.2 Cosine term

The cosine terms in the flow profile equation (2.2.12) can be solved analytically as well, since $\bar{\omega}$ is always multiplied by α, $\sqrt{\alpha\bar{\omega}}$ is substituted by Ω, the integration of the cosine terms then result in:

$$\int_0^1 \frac{\cos\left(\sqrt{\alpha\bar{\omega}}(1-\bar{y})\right)}{\cos(\sqrt{\alpha\bar{\omega}})} d\bar{y} = \int_0^1 \frac{\cos\left(\Omega(1-\bar{y})\right)}{\cos(\Omega)} d\bar{y} = \operatorname{tanc}(\Omega) \text{ [–]} \tag{3.1.5}$$

Where tanc is the defined by analogy with the sinc function[1]: $\operatorname{tanc}(x) = \begin{cases} 1 & \text{if } x = 0 \\ \frac{\tan(x)}{x} & \text{if } n \neq 0 \end{cases}$ which can not be simplified any further.

[1] Wolfram

3.1.3 Volumetric flow density

The simplified integrals (3.1.4) and (3.1.5) are used to evaluate the normalized flow density (2.4.2) and results in:

$$\begin{aligned} Q^*(\omega) &= \int_0^1 \left(\frac{1-i\omega^*}{\alpha\bar{\omega}}\right)\left(1-\frac{\cos\left(\sqrt{\alpha\bar{\omega}}(1-\bar{y})\right)}{\cos\left(\sqrt{\alpha\bar{\omega}}\right)}\right) \\ &\quad + \bar{E}_s(\omega)\frac{1-i\omega^*}{1+\alpha\bar{\omega}\bar{\lambda}^2}\left(e^{-\bar{y}/\bar{\lambda}}-\frac{\cos\left(\sqrt{\alpha\bar{\omega}}(1-\bar{y})\right)}{\cos\left(\sqrt{\alpha\bar{\omega}}\right)}\right)d\bar{y} \\ &= \left(\frac{1-i\omega^*}{\Omega^2}\right)(1-\operatorname{tanc}(\Omega)) + \bar{E}_s(\omega)\frac{1-i\omega^*}{1+\Omega^2\bar{\lambda}^2\diamond}\left(\bar{\lambda}-\operatorname{tanc}(\Omega)\right)\ [-] \end{aligned} \tag{3.1.6}$$

Since the resonance frequency is always around $1/\sqrt{\alpha}$, Ω will always be in the order of 1. $\bar{\lambda}^2$ will always be smaller than 0.01 and therefore the term $\Omega^2\bar{\lambda}^2 << 1$ and thus will be neglected.

3.1.4 Streaming potential

In the streaming potential description (2.3.13) three integrals are present: ι_1, ι_2 and ι_3, describing the streaming (ι_1 and ι_2) and conduction (ι_3) current. The first two can not be solved analytically and will therefore be linearised (so, $\bar{\psi}(\bar{y}) = e^{\bar{y}/\bar{\lambda}}$ is assumed). ι_1 is represents the current caused by the movement of the liquid and therefore creates part of the streaming current:

$$\begin{aligned} \iota_1(\omega^*) &= \frac{1-i\omega^*}{\Omega^2}\int_0^1\left(1-\frac{\cos(\Omega(1-\bar{y})}{\cos(\Omega)}\right)\bar{\psi}(\bar{y})d\bar{y} \\ &= \frac{\bar{\lambda}(1-i\omega^*)}{\Omega^2}\frac{\cos(\Omega)\left(\Omega^2\bar{\lambda}^2-e^{-1/\bar{\lambda}}\diamond-\Omega^2\bar{\lambda}^2\,e^{-1/\bar{\lambda}}\diamond\right)-\bar{\lambda}\Omega\sin(\Omega)+e^{-1/\bar{\lambda}}\diamond}{\cos(\Omega)(1+\Omega^2\bar{\lambda}^2\diamond)}\ [-] \end{aligned} \tag{3.1.7}$$

In the numerator of (3.1.7) some terms can be neglected: $\Omega^2\lambda^2 e^{-1/\bar{\lambda}} << e^{-1/\bar{\lambda}} << \Omega^2\lambda^2$ and therefore only the former ($\Omega^2\bar{\lambda}^2$) term is taken into account. The exponential term is also negligible: $e^{-1/\bar{\lambda}} << \cos(\Omega)\Omega^2\bar{\lambda}^2 - \bar{\lambda}\Omega\sin(\Omega)$ and will be discarded. Regarding the denominator the same arguments as for (3.1.6) hold and the $\Omega^2\bar{\lambda}$ term will be neglected as well.

The $\cosh$ term in (2.2.12) is caused by the double layer potential, so it will be replaced by (3.1.3), the linearized double layer potential. ι_2 is an integral which takes account for the flow in opposite direction of the pressure gradient and the implications to the streaming potential. The simplification arguments of

(3.1.7) are applied to (3.1.8) as well:

$$\begin{aligned}\iota_2(\omega^*) &= \frac{1-i\omega^*}{1+\Omega^2\bar{\lambda}^2}\int_0^1\left(\psi(\bar{y})-\frac{\cos(\Omega(1-\bar{y})}{\cos(\Omega)}\right)\bar{\psi}(\bar{y})d\bar{y} \\ &= -\lambda(1-i\omega^*)\frac{\cos(\Omega)\left(\frac{1}{2}+\frac{1}{2}e^{-2/\bar{\lambda}}\diamond+\frac{1}{2}\Omega^2\bar{\lambda}^2e^{-2/\bar{\lambda}}\diamond-\frac{1}{2}\Omega^2\bar{\lambda}^2\diamond\right)+\Omega\lambda\sin(\Omega)-e^{-1/\bar{\lambda}}\diamond}{\cos(\Omega)(1+\Omega^2\lambda^2\diamond)^2}\ [-]\end{aligned} \tag{3.1.8}$$

Disregarding these terms results in the following simplifications for ι_1 and ι_2:

$$\begin{aligned}\iota_1(\omega^*) &\approx \bar{\lambda}(1-i\omega^*)\left(\bar{\lambda}^2-\bar{\lambda}\operatorname{tanc}(\Omega)\right) \\ &= \bar{\lambda}(1-i\omega^*)\left(\bar{\lambda}^2-\bar{\lambda}\operatorname{tanc}\left(\sqrt{\alpha\omega^*(i+\omega^*)}\right)\right)\ [-]\end{aligned} \tag{3.1.9}$$

$$\begin{aligned}\iota_2(\omega^*) &\approx -\bar{\lambda}(1-i\omega^*)\left(\frac{1}{2}+\bar{\lambda}\Omega\tan(\Omega)\right) \\ &= -\bar{\lambda}(1-i\omega^*)\left(\frac{1}{2}+\bar{\lambda}\sqrt{\alpha\omega^*(i+\omega^*)}\tan\left(\sqrt{\alpha\omega^*(i+\omega^*)}\right)\right)\ [-]\end{aligned} \tag{3.1.10}$$

The third integral, ι_3, describing the conduction current is defined as:

$$\begin{aligned}\iota_3 &= \int_0^1\cosh(\bar{\zeta}\bar{\psi}(\bar{y}))d\bar{y} \\ &= \bar{\lambda}\left(\operatorname{Chi}\left(\bar{\zeta}\right)-\operatorname{Chi}\left(\bar{\zeta}e^{-1/\bar{\lambda}}\right)\right)\ [-]\end{aligned} \tag{3.1.11}$$

Where Chi is the hyperbolic cosine integral function $\operatorname{Chi}(x)=\gamma+\ln(x)+\int_0^x\frac{\cosh(t)-1}{t}dt$, where γ is the Euler-Mascheroni constant (≈ 0.577)[2]. The first order Taylor approximation of (3.1.11) around $x=0$ for large a is: $\operatorname{Chi}(x)-\operatorname{Chi}(ax)\approx-\ln(a)$ [3]. Since $|\bar{\zeta}|<1$ and $\bar{\lambda}<0.1\Rightarrow e^{-1/\bar{\lambda}}<4\times10^{-5}$, the following can be assumed: $\iota_3\approx-\bar{\lambda}\ln(e^{-1/\bar{\lambda}})=\bar{\lambda}/\bar{\lambda}=1$.

The streaming potential can now be described as a closed function of Ω or ω^*, only depending on J,

[2] NIST
[3] WolframAlpha

Du, $\bar{\lambda}$ and α:

$$\begin{aligned}\bar{E}_s(\omega^*) =& \frac{\iota_1(\omega^*)}{\iota_2(\omega^*)+J(\iota_3+Du)} \\ \approx& -\frac{\bar{\lambda}(1-i\omega^*)\left(\bar{\lambda}^2-\bar{\lambda}\,\mathrm{tanc}(\Omega)\right)}{\bar{\lambda}(1-i\omega^*)\left(\frac{1}{2}+\bar{\lambda}\Omega\tan(\Omega)\right)+J(1+Du)} \\ =& -\frac{\bar{\lambda}(1-i\omega^*)\left(\bar{\lambda}^2-\bar{\lambda}\,\mathrm{tanc}\left(\sqrt{\alpha\omega^*(i+\omega^*)}\right)\right)}{\bar{\lambda}(1-i\omega^*)\left(\frac{1}{2}+\bar{\lambda}\sqrt{\alpha\omega^*(i+\omega^*)}\tan\left(\sqrt{\alpha\omega^*(i+\omega^*)}\right)\right)+J(1+Du)}\ [-]\end{aligned} \tag{3.1.12}$$

Where J the ratio of streaming versus conduction current and Du the Duhkin number describing the surface conduction.

3.1.5 Efficiency from normalized parameters

The efficiency has be defined in 2.3.1 as $\eta_{eff} = \frac{P_{elec}}{P_{hydr}} = \frac{<I_c(\omega)E_s(\omega)>_t}{<\frac{dP(x,\omega)}{dx}Q(\omega)>_t}$ using the known normalization relations from page 11 all terms are made non dimensional:

$$\begin{aligned}\eta_{eff}(\omega) =& \frac{E_s(\omega)I_c(\omega)}{\frac{dP(x,\omega)}{dx}Q(\omega)} \\ =& \frac{\bar{E}_s\frac{dP(x,\omega)}{dx}H^2}{\epsilon\zeta}\,\frac{\sigma_b\bar{E}_s\frac{dP(x,\omega)}{dx}H^2\iota_3}{\epsilon\zeta}\,\frac{1}{\frac{dP(x,\omega)}{dx}}\,\frac{\eta}{H^2\frac{dP(x,\omega)}{dx}Q^*(\omega)} \\ =& \frac{H^2\sigma_b\eta\iota_3}{\epsilon^2\zeta^2}\frac{\bar{E}_s^2(\omega)}{Q^*(\omega)} \\ =& \frac{J\iota_3}{\bar{\lambda}^2}\frac{\bar{E}_s^2(\omega)}{Q^*(\omega)} \\ \approx& \frac{J}{\bar{\lambda}^2}\frac{\bar{E}_s^2(\omega)}{Q^*(\omega)}\ [-]\end{aligned} \tag{3.1.13}$$

This relation can be used easier, since it uses dimensionless numbers and can therefore be used in a vast range of systems. However, it is advisable to convert the dimensionless numbers back to real numbers, so one knows in what order of magnitude the results are.

3.2 Actual parameter values

In order to make all the integrals which are calculated make sense, it is necessary to convert them back into real world parameters and units. First, the streaming potential is revered using the relations on page

11:

$$E_s(\omega^*) = \bar{E}_s(\omega^*)\frac{\frac{\partial p(x,\omega^*)}{\partial x}H^2}{\epsilon\zeta}\ [\text{V/m}] \tag{3.2.1}$$

The streaming current density is a function of the normalized streaming potential ($\bar{E}_s(\omega^*)$), $\iota_1(\omega^*)$ and $\iota_2(\omega^*)$. It is transformed back to amperes by dividing it by the normalization constant ($C_{norm} = J\frac{\epsilon\zeta}{\frac{dp}{dx}H^2}\frac{1}{\sigma_b}$, for more information: (B.1.3)) used in section B.1:

$$I_s(\omega^*) = \frac{\iota_1(\omega^*) + \bar{E}_s(\omega^*)\iota_2(\omega^*)}{C_{norm}}\ [\text{A/m}^2] \tag{3.2.2}$$

ι_3 is found to be approximately 1 and therefore I_c becomes relatively easy and intuitively, namely: a conductance times a electrical field:

$$I_c(\omega^*) = \frac{J\bar{E}_s(\omega^*)\iota_3}{C_{norm}} \approx \sigma_b E_s(\omega^*)\ [\text{A/m}^2] \tag{3.2.3}$$

Also, the Dukhin current density has a sensible relation, since the Dukhin number is defined as a factor of the conduction current it also appears as a fraction of the conduction current in the equations:

$$I_{Du}(\omega^*) = \frac{J\bar{E}_s Du}{C_{norm}} = \sigma_b E_s(\omega^*)Du \approx I_c(\omega^*)Du\ [\text{A/m}^2] \tag{3.2.4}$$

The non dimensional flow profile can be scaled back to the actual flow profile using the following relationship:

$$U(y,\omega^*) = U^*(y/H,\omega^*)\frac{\frac{\partial P(x,\omega^*)}{\partial x}H^2}{\eta}\ [\text{m/s}] \tag{3.2.5}$$

Subsequently the actual volumetric flow density can be found by multiplying $Q^*(\omega^*)$ by the same factor as $U^*(\bar{y},\omega^*)$:

$$\bar{Q}(\omega^*) = Q^*(\omega^*)\frac{\frac{\partial P(x,\omega^*)}{\partial x}H^2}{\eta}\ [\text{m/s}] \tag{3.2.6}$$

3.3 Reynolds number

In the The Reynolds number is a dimensionless number which indicates the ratio of inertial forces over viscous forces and points out whether a flow will behave laminar or turbulent. It is defined as[17]:

$$Re = \frac{\rho u_{mean} L}{\eta} \; [-] \tag{3.3.1}$$

where ρ [kg/m^3] is the density, u_{mean} [m/s] the mean velocity of the fluid, L [m] a characteristic length and η [Pa s] the dynamic viscosity. For two parallel plates the characteritic length is $_4H$, with H [m] the half height of the channel. The mean velocity is equal to the volumetric flow density $u_{mean}(\omega^*) = Q(\omega^*)$ [m/s]. The dynamic viscosity is η, but since a viscoelastic fluid is used, the viscosity is frequency dependent. Using the Maxwell model this results in the frequency dependent viscosity: $\eta(\omega^*) = \eta_0 \frac{1}{1+\omega^{*2}}$ [26].

During the derivation of the equations of Bandopadhyay, a low Reynolds number is assumed, so a laminar flow can be assumed. This will be checked in the results.

3.4 Non constant J

In Bandopadhyays work, it is assumed that the factor J (the ratio of streaming current and conduction current) is constant with changing α and ω^*. However, α is dependent on the zero shear viscosity η_0 ($\alpha = \frac{\rho H^2}{\eta_0 t_m}$), J is also dependent on the viscosity ($J = -\frac{\sigma_b \eta \lambda^2}{\epsilon^2 \zeta^2}$) so it can change if α changes. Bandopadhyay based his five α's on two zero shear viscosities ($\eta_0 = 1 \times 10^{-3}$ and 1×10^{-2} Pa s) and three time constants ($t_m = 1 \times 10^{-4}$, 1×10^{-3} and 1×10^{-2} s). These α's are calculated in table 3.4.1, assuming $H = 100 \times 10^{-9}$ m and $\rho = 1 \times 10^3$ kg/m^3. Also, J is calculated, assuming the conductivity of blood $\sigma_b = 0.67$ S/m [27], $\lambda = 10 \times 10^{-9}$ m, $\epsilon = 80 \times 8.9 \times 10^{-12}$ F/m and $\zeta = 25$ mV, resulting in $J_0 = 210 \times 10^3 \eta_0$. It can be seen that the factor J_0 is more than a factor of ten higher than assumed in Bandopadhyay's paper.

Table 3.4.1: Comparisson of J and α, with Bandopadyay's parameters, except for the first three rows (marked with a *), which are added for comparison

t_m/s	η_0/Pa s	α/–	J/–
1×10^{-8}*	1×10^{-3}	1	-2.1×10^2
1×10^{-6}*	1×10^{-3}	1×10^{-2}	-2.1×10^2
2×10^{-3}*	5×10^{-5}	1×10^{-4}	-1.1×10^1
1×10^{-4}	1×10^{-3}	1×10^{-4}	-2.1×10^2
1×10^{-3}	1×10^{-3}	1×10^{-5}	-2.1×10^2
1×10^{-4}	1×10^{-2}	1×10^{-5}	-2.1×10^3
1×10^{-3}	1×10^{-2}	1×10^{-6}	-2.1×10^3

Since the viscosity changes with frequency, J could also change with frequency. The factor is defined as a ratio between the a reference conduction current and a reference streaming current. In Newtonian fluids these currents will also change with frequency, having a cut off frequency of $\frac{8\eta}{H^2\rho}$ in capillaries [9]. However, this is not further investigated.

3.5 Dukhin number

Until now, the Dukhin number is not taken into account in all calculations (as it was set to 0). The Dukhin number is a dimensionless number indicating the ratio between surface conduction and bulk conduction and is defined as $Du = \sigma_s/\sigma_b H$, where σ_s [S] is the surface conductivity [28, 29]. According to several sources [28, 14, 30] the specific surface conductance of a glass-water interface is 1×10^{-9} S to 5×10^{-9} S meaning that in order to neglect the surface conductance (say, $Du < 0.05$):

$$H_{min} > \frac{\sigma_s}{Du_{max}\sigma_b} = 1 \times 10^{-7}/\sigma_b \text{ [m]} \tag{3.5.1}$$

3.6 Estimation of the optimal frequency

The efficiency is calculated from the dimensionless parameters using (3.1.13): $\frac{J}{\bar{\lambda}^2}\frac{\bar{E}_s^2(\omega)}{Q^*(\omega)}$ and since J and $\bar{\lambda}$ are system parameters, the optimal frequency of the system occurs at either a high $\bar{E}_s$ (high output power) or a low Q^* (low input power). If the real part of the denominator of $\bar{E}_s$ is zero, $\bar{E}_s$ will be highest. Recalling 3.1.12, the denominator is given by: $\bar{\lambda}(1 - i\omega^*)\left(\frac{1}{2} + \bar{\lambda}\Omega\tan(\Omega)\right) + J(1 + Du)$ and the real part will be zero if:

$$\Omega\tan(\Omega) = \frac{-J(1 + Du) - \frac{1}{2}\bar{\lambda}}{\bar{\lambda}^2} \text{ [–]} \tag{3.6.1}$$

In the case of Bandopadyhyays assumptions ($\bar{\lambda} = 1/10$, $J = -10$ and $Du = 0$), this would result in $\Omega\tan(\Omega) = 995$ and is shown graphically in figure 3.6.1a, generally $\bar{\lambda}$ will be smaller and both J and Du higher than these assumptions, therefore this number (995) will only become higher. Since $\tan(x)$ has asymptotes at $x = \frac{2k-1}{1}\pi$, it can be assumed that at $\Re\mathfrak{e}(\Omega) \approx \frac{2k-1}{2}\pi$, with $k = 1, 2, 3, \ldots$ the streaming potential will be highest. But, the simplifications made in the previous sections assumed that Ω was in the order of 1 and therefore $k = 0$ will be taken as the frequency for the highest streaming potential.

The lowest flow will occur if the real part of the numerator of (3.1.6) is (almost) zero. This will be the

case if

$$1 - \mathrm{tanc}(\Omega) = \bar{E}_s(\Omega)(\Omega^2 \bar{\lambda} - \Omega \tan(\Omega)) \; [-] \tag{3.6.2}$$

. This cannot be solved analytically, so it is plotted in figure 3.6.1b. It can be seen that despite the fact that the streaming potential has its first maximum around $\pi/2$, the first minimum for the flow is near $3\pi/2$. Which can explain why there are double peaks after the first single efficiency spikes in figure 2.5.1a. A problem with a high efficiency because of a very low flow is that, although the efficiency is high, due to the low input power the output power will also be very low. So these peaks will not be used in further analysis.

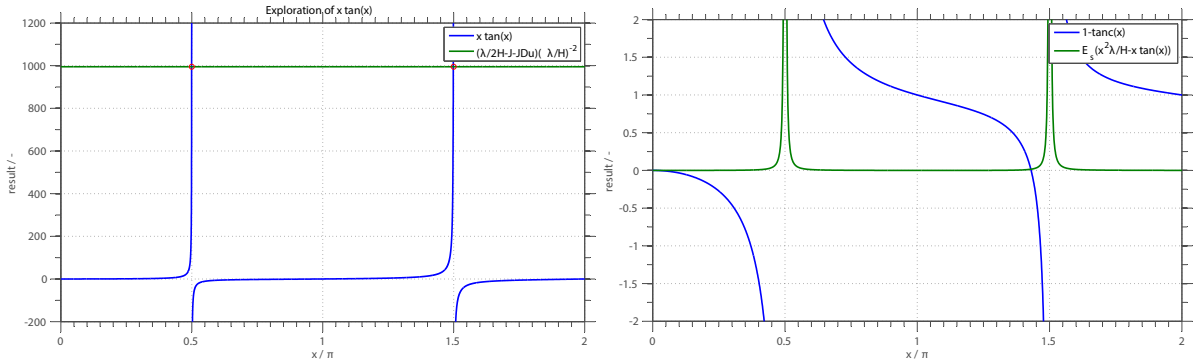

(a) $x\tan(x)$ plotted as multiple of π

(b) Graphical representation of $1 - \mathrm{tanc}(\Omega) = \bar{E}_s(\Omega)(\Omega^2 \bar{\lambda} - \Omega \tan(\Omega))$, with $\bar{\lambda} = 1/10, J = -10$ and $Du = 0$

Figure 3.6.1: Graphical representation of $x\tan(x)$ and $1 - \mathrm{tanc}(x)$

3.7 Viscoelastic fluids

During this project viscoelastic fluids are concerned. Lots of viscoelastic fluids exist, the fluids which will be used in this project need to have three main properties: a low conductivity (so it needs to be non-ionic) to get a large Debye length; also, it needs to have a long relaxation time, which will result in low resonance frequencies and low alpha's; but, a low viscosity so it will easily flow into the channel and the resonance frequency will be low as well. Therefore nonionic 'living polymer' solutions will be used, which can be tuned by changing the concentration of the surfactants and additives [18, 31, 32].

3.8 Scaling problem

The conversion efficiency can be optimized in several ways: from a mechanical and manufacturing point of view it would be optimal to work in low frequency ranges and large channels (easy to manufacture)

with liquids which have a low viscosity (so it is easy to (re)fill the device). But, for a high efficiency a low α is needed and also $\bar{\lambda}$ must not be too small. Therefore the height of the channel should be as low as possible. Also the J parameter should be as small as possible, requiring a high conductivity (high salt concentration) and a low Debye-length (low salt concentration) which results in an undesirable small $\bar{\lambda}$.

Table 3.8.1: Dependencies of different parameters

Parameter	α	$\bar{\lambda}$	J	ω_r	Du	range
Relation	$\frac{\rho H^2}{\eta t_m}$	$\sqrt{\frac{\epsilon k_B T}{H^2 z^2 e^2 n_0}}$	$-\frac{\sigma_b \eta \lambda^2}{\epsilon^2 \zeta^2}$	$\frac{\pi\sqrt{\eta}}{H\sqrt{\rho t_m}}$	$\frac{\sigma_s}{\sigma_b H}$	
Optimum	$\to 0$	$\to \infty$	$\to 0$	$\to 0$	$\to 0$	
$H\diamond$	$\to 0$	$\to 0$		$\to \infty$	$\to \infty$	$100\,\text{nm} - \infty\text{m}$
$\lambda\diamond$		$\to \infty$	$\to 0$			$0.10\,\text{nm} - 1000\,\text{nm}$
η	$\to \infty$		$\to 0$	$\to 0$		$1\times10^{-4}\,\text{Pa s} - 100\,\text{Pa s}$[17, 31]
$t_m \propto \eta\diamond$	$\to \infty$			$\to \infty$		$<< 1\,\text{ms} - 10\,\text{s}$
$\sigma_b \propto n_0\diamond$		$\to 0$	$\to 0 \& \to \infty$		$\to \infty$	$5.5\times10^{-6}\,\text{S/m}$[33]$-10\,\text{S/m}$
$\rho\diamond$	$\to 0$			$\to \infty$		$\approx 1\times10^{3}\,\text{kg/m}^3$[17]
$\epsilon \propto \epsilon_r$		$\to \infty$	$\to \infty$			$(\epsilon_r =) 1\,\text{F/m} - 190\,\text{F/m}$[17]
$\lvert\zeta\rvert$			$\to \infty$			$1\,\text{mV} - 100\,\text{mV}$[11]

In table 3.8.1 the dependencies of all parameters are shown, the range in which they can be tuned is also given. Conflicting parameters are shown in red and denoted with a diamond ($\diamond$), whereas non-conflicting are marked green.

Starting with the non conflicting parameters: the ζ-potential has to be as high as possible. However, the proposed models only hold for low ζ-potentials so it could make the system working less effective as well. Secondly, the permittivity, ϵ_r, should be as high as possible. However, water already has a permittivity of $80\,\text{F/m}$ so the permittivity can only be increased by a factor of two. The relaxation time of the liquid should also be as high as possible, resulting in a low operating frequency and a low inverse Deborah number (α). A downside is that the relaxation time is related to the viscosity: one can imagine that if it takes a long time for a liquid to relax it will be very viscous as well.

For the red parameters it is easiest to start with ρ, since it can not change very much it can not be optimized. The maximum height H is given by λ, since the Debye length cannot be larger than $1\,\mu\text{m}$ in water (ultra pure water has a pH of 7, so the concentration of ions is at least $1\times10^{-7}\,\text{mol/L}$, thus $\lambda_{max} = \frac{0.304}{\sqrt{1\times10^{-7}}} \approx 1\,\mu\text{m}$). However, additives are needed to make water viscoelastic, so the Debye length will always be smaller than $1\,\mu\text{m}$.

Then, the conductivity is an even harder nut to crack: in order to get a large Debye length, the salt concentration should be as low as possible and thus the conductivity. Also for a low J a low conductivity is preferred, but also a small Debye length. A very low conductivity will in the end be counteracted by the surface conduction, so a minimum height is needed as well. Since a large normalized Debye length is

preferred in general, the conductivity has be as low as possible (5.5×10^{-6} S/m in water).

As a low α is needed to get a high efficiency, the viscosity should be high, however a high viscosity results in a high driving frequency which is not very convenient using a high viscosity liquid. The J parameter should be as low as possible and therefore the viscosity needs to be as low as possible as well. In contrast to α and ω_r, the J parameter is dependent on the frequency dependent since the streaming potential and thus the conduction current will increase with higher viscosities see section B.1.

3.9 Addition of a load resistance

The work of Bandopadhyay and Chakraborty [10] is focussed on the conversion of hydrodynamic energy into electrical energy. Whereas this thesis is aimed to use the hydrodynamic energy to power an external device. In order to do that, an external load has to be added into the equations. This external load will not affect the velocity profile substantially, but it will effect the electrical potential, which will become lower due to the decrease of electrical resistance between both ports of the device. Also, the analysed current will be the current through the load in stead of the conduction current (which therefore becomes a loss factor). Kirchoff's current law in (B.1.1) is expanded to:

$$A(I_s + I_c + I_{Du} + I_l) = 0 \text{ [A]} \tag{3.9.1}$$

where $I_l = E_s/\rho_l$ is the current density trough the load (which area and length is defined equal to that of the device, so $\rho_l = R_{load}L/A$), with the load resistivity ρ_l [Ω/m]. Following the procedure in section B.1 it follows that:

$$\bar{E}_s = \frac{-\iota_1}{\iota_2 + J(\iota_3 + Du + \iota_4)} \text{ [–]} \tag{3.9.2}$$

where $\iota_4 = \frac{1}{\sigma_b \rho_L}$ [–] is the non-dimensional current density trough the load and $I_l = \frac{\sigma_b \bar{E}_s \iota_4}{C_{norm}}$ A/m^2.

The efficiency is then defined as the current trough the load times the streaming potential over the hydraulic input power:

$$\eta_{load} = \frac{\tilde{E}(\omega^*) I_l(\omega^*)}{\frac{dP}{dx} Q(\omega^*)} = \frac{J \iota_4 \bar{E}_s^2(\omega^*)}{\bar{\lambda}^2 Q^*(\omega^*)} \text{ [–]} \tag{3.9.3}$$

Jacobi's law (1840) states that the maximum power transfer is achieved if the resistance of the source is equal to the resistance of the load. This case if $R_c = R_l$ and is depicted in figure 3.9.1. Until 1880 it was thought that this was also the maximum power transfer efficiency. However, Edison then found that

the maximum power transfer efficiency is achieved (in the case of a current source) if the load resistor is much higher than the source resistor, for more information, see appendix C.

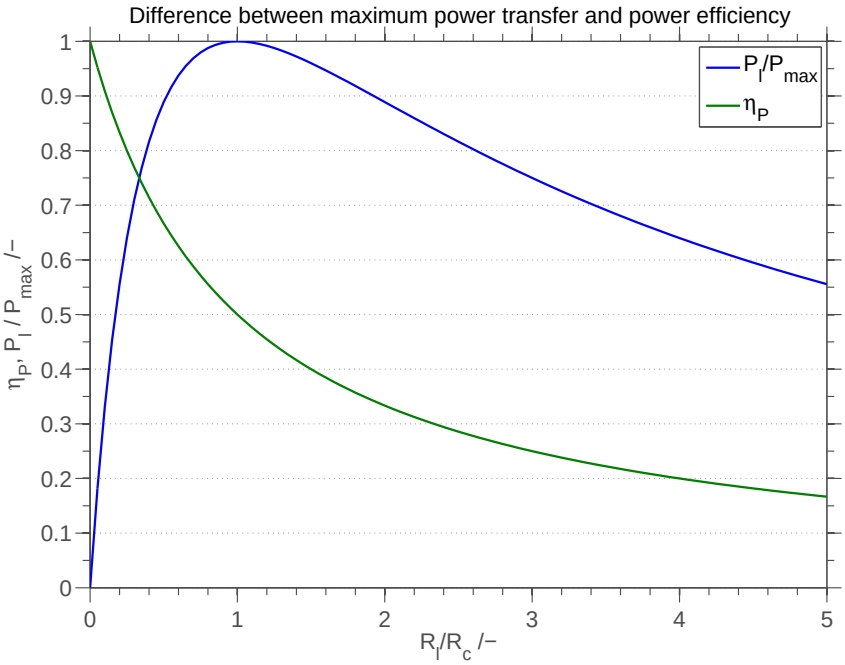

Figure 3.9.1: Jacobi's law (in blue) and the power efficiency (in green).

Therefore a trade-off has to be made in order to get either a high power or a high efficiency. So the resistivity of the load resistor should be lower or at most equal to the resistivity of the channel.

3.10 Flowprofile

In figure 3.10.1 the flowprofile in the channel is given for different α's, the double layer potential ($\bar{\psi}$) is plotted as well in order to show the effect of the flow velocity at different $\bar{y}$'s since the streaming current is caused by the integral of the double layer times the flow velocity. A alternating pressure is applied from top to bottom. The profiles are normalized such that the maximum flow is one.

In figure 3.10.1a a very low frequency is modelled ($\omega^* \sqrt{\alpha} = 1 \times 10^{-8}$) and the profile has the same shape for all α's, so only the first is shown. It can be seen that the out of phase part ($\mathfrak{I}$) of the flow is almost zero and the main part of the flow is caused by the in phase ($\mathfrak{R}$) pressure driven part U_p^* in (2.2.13). The electro-viscous part U_E^* is close to zero as well.

The figures 3.10.1b to 3.10.1f are created at the frequency where the highest conversion energy is available for that α so $\omega^* \approx \pi/2\sqrt{\alpha}$. It can be seen that each α behaves differently.

A relatively high α (figure 3.10.1b, $\alpha = 1$) results in a relative increase of the out of phase part, the electro-viscous effect is still negligible. If α is decreased to 1×10^{-2} (figure 3.10.1c) the out of

phase parts begin to increase and the electro viscous effect (green) starts to play a significant role in counteracting the pressure driven flow (blue) resulting in a lower net flow (red). One can observe that the profile of the electro viscous effect is not as it is in Newtonian liquids with a constant pressure gradient, in that case it would be a flat plug profile with smooth edges at the channel walls, as in figure 1.1.2.

In the next plot, figure 3.10.1d, it can be seen that the out of phase parts begin to increase, but almost cancel out each other. An other peculiar phenomenon is that the electro viscous effect is getting most significant for the total flow. And it is in an unexpected direction (it should counter-act the pressure driven flow).

In the final two plots, figures 3.10.1e and 3.10.1f the out of phase flow decreases, but the in phase flow even becomes negative at the edges and positive in the middle (relative to the applied pressure). This will have a extensive influence on the calculation of the input power, which will be explained in the next section.

3.11 Definition of the input power

The input power is poorly defined: it is defined as the integral of the flow profile, which indeed represents a flow. However, as became clear in figures 3.10.1e and 3.10.1f the flow profile can be both negative and positive at the same time at different locations. And since the phase information will be lost in the calculation of the efficiency anyway, the volumetric flow density should be calculated as: $\bar{Q}^* \int_0^1 |U^*(\bar{y}, \omega^*)| d\bar{y}$.

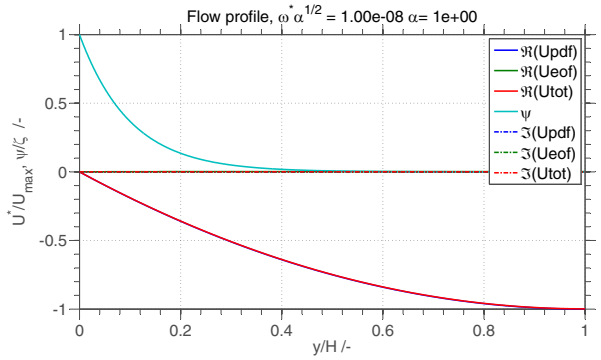

(a) Low frequency (DC) flow profile, which is the same for all different α's

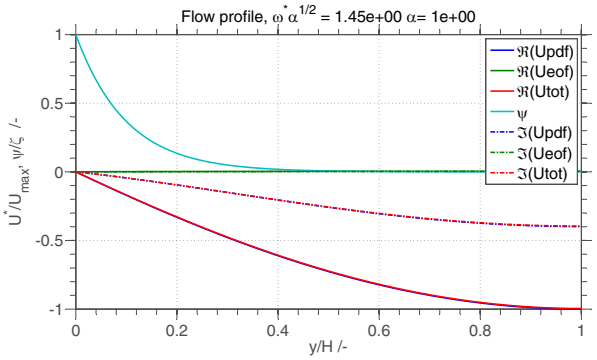

(b) The flowprofile at the maximum conversion efficency for $\alpha = 1$

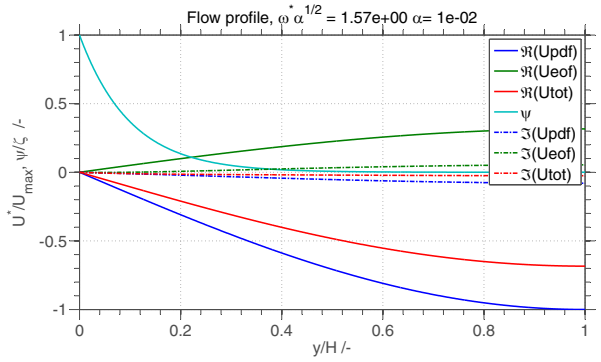

(c) The flowprofile at the maximum conversion efficency for $\alpha = 1 \times 10^{-2}$

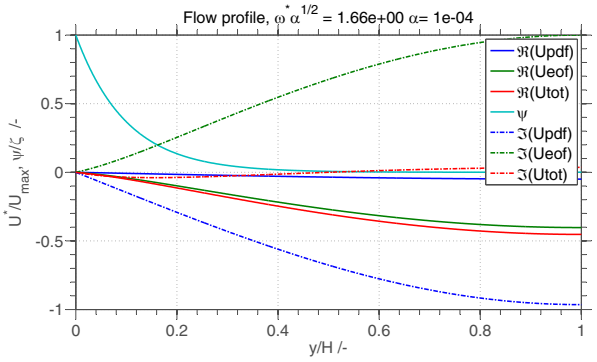

(d) The flowprofile at the maximum conversion efficency for $\alpha = 1 \times 10^{-4}$

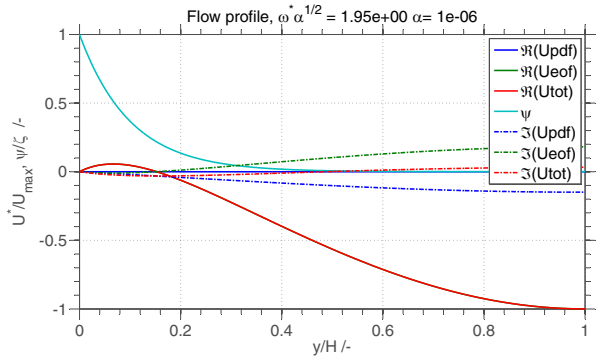

(e) The flowprofile at the maximum conversion efficency for $\alpha = 1 \times 10^{-6}$

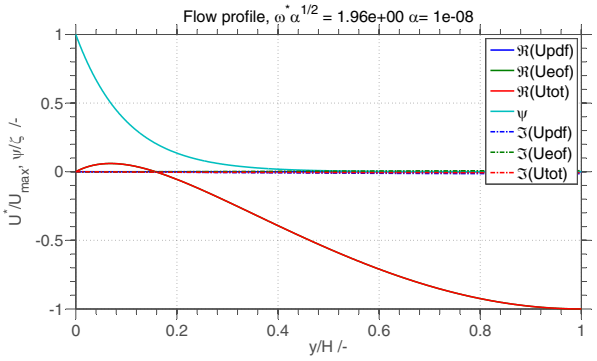

(f) The flowprofile at the maximum conversion efficency for $\alpha = 1 \times 10^{-8}$

Figure 3.10.1: Flowprofiles at the different frequencies with changing α, with the parameters $\bar{\lambda} = 1/10$, $Du = 0$ and $J = -10$

4 Method

During all theoretical work a setup is constructed as well. The ultimate design is taken as a starting point and gradually adapted into a more feasible design for a eight month project. Unfortunately no experiments were conducted.

4.1 Ultimate setup

The ultimate setup would have the following properties:

No loss between pump and device

No noise (from the pump) into the device

No loss from current pick up

Frequency range Hz-MHz

Pressure actuated

Easy to change parameters

4.2 Realized design

Although the optimal design is not feasible to realize in seven months, a simpler setup is realized. The setup consists of a small disposable microfluidic pump, a 2.5 cm capillary and two platinum electrodes and is depicted in figure 4.5.1a.

4.2.1 Pump

The used pump is a BARTELS MIKROTECHNIK MP5, this pump consists of a channel which has a chamber with a piezoelectric actuator on top of it, connected by a small hole. The channel normally has valves for an unidirectional flow, but they are removed. A schematic overview of the working principle is given in figure 4.2.1.

4.2.2 Electronics

The pump needs to be driven by a voltage source capable of driving frequencies between 0 and 300 Hz and voltages between 0 and 250 V. These signals will be created by a voltage source which will be connected to the jack plug attached to the pump.

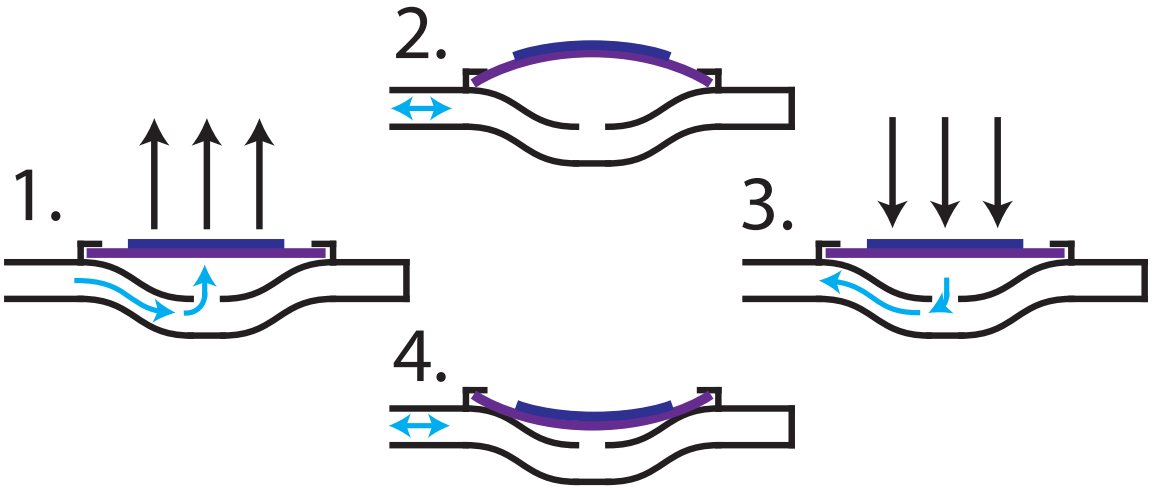

Figure 4.2.1: **Working principle of the micropump** 1. The piezoelectric material expands, so the pumping chamber becomes larger and liquid will flow in. 2. At the maximum volume, the potential over the piezoelectric material will decrease and the chamber will shrink. 3. The liquid flows back. 4. The chamber is emptied and the voltage will increase. One cycle is finished. Picture is adapted from www.bartels-mikrotechnik.de

The generated streaming current will be collected capacitively by two platinum wires. In order to do that, the frequency needs to be higher than the cut-off frequency f_{co}, which is dependent on the electrical resistance of the liquid in the capillary (R_{cap}) and the double layer capacitance of the platinum wires (C_{dl}).

$$f_{co} = \frac{1}{2\pi R_{cap} C_{dl}} = 26.9 \text{ [µHz]} \tag{4.2.1}$$

4.2.3 Parameters

The parameters of the setup and for the experiments are listed in table 4.2.1

4.3 Analysis

To make an analysis, MilliQ water (Newtonian liquid) experiments are compared with water with added sucrose palmitate ($P1695$ in [31]) and Brij™ L4 ($C_{12}EO_4$[31]) experiments.

4.4 Chemicals

In table 4.4.1, the used chemicals are listed.

Table 4.2.1: Summary of the device parameters

Parameter	Symbol	Equation	Value
Capillary radius	r		35 µm
Capillary length	L		2.5 cm
Capillary volume	V_{cap}	$V = \pi r^2 L$	0.096 µL=0.096 mm^3
Pumping volume (5 V to 250 V)	V_{pump}		0.016 µL to 0.83 µL=0.016 mm^3 to 0.83 mm^3
Total volume	V_{tot}		28 µL=28 mm^3
Dead volume	V_{dead}	$V_{tot} - V_{pump}$	28 µL to 27 µL=28 mm^3 to 27 mm^3
Electrode radius	r_{elec}		0.10 mm
Electrode length	L_{elec}		5 mm
Surface charge	σ_q		0.20 F/m^2
Liquid conductivity	σ_b		6.9 µS/cm=690 µS/m
Electrical resistance capillary	R_{cap}	$\frac{L}{\sigma_b \pi r^2}$	9.4 GΩ
Double layer capacitance	C_{dl}	$\sigma_q L_{elec} 2\pi r_{elec}$	0.63 µF
Compressibility (Air; water)	K		1×10^{-5} and 4.6×10^{-10} 1/Pa
Viscosity (Air; water and VE)	η		0.018, 1 and 100 mPa s
Relaxation time (Water and VE)	t_m		1×10^{-6} and 0.10 s

Table 4.4.1: Used chemicals during the experiments including their concentration and supplier.

Chemical	Solvent	Concentration	Supplier
Water (H_2O)	âĂć	âĂć	âĂć
Brij™ L4 (Polyoxyethylene (4) lauryl ether)	âĂć	âĂć	Sigma Aldrich
Sucrose Palmitate ($C_{28}H_{52}O_{12}$)	âĂć	âĂć	Carbosynth

4.5 Filling of the device

Finding a method to fill the device was quite a challenge. The device can be filled with the use of a vacuum and capillary forces. MEDIMATE B.V. had offered to help to fill the device, however the vacuum pump was broken during the filling and at the time it was fixed no time was left to perform the measurements.

The device is inserted into a vacuum vessel, which is connected to a vacuum pump and evacuated. At the top a liquid containing vessel is connected by a tap, which will be opened when the bottom vessel and the measurement setup are evacuated, as is depicted in figure 4.5.1b. The liquid will enter the device by capillary forces and, if the vacuum is removed, by an extra pressure difference of ≈ 1 bar.

4.5.1 Evacuation time

The system consists of two hydraulic resistances: the capillary and the pump. Since the capillary radius is a lot smaller than the pump thickness ($r << t$), its hydraulic resistance is most significant. And is given

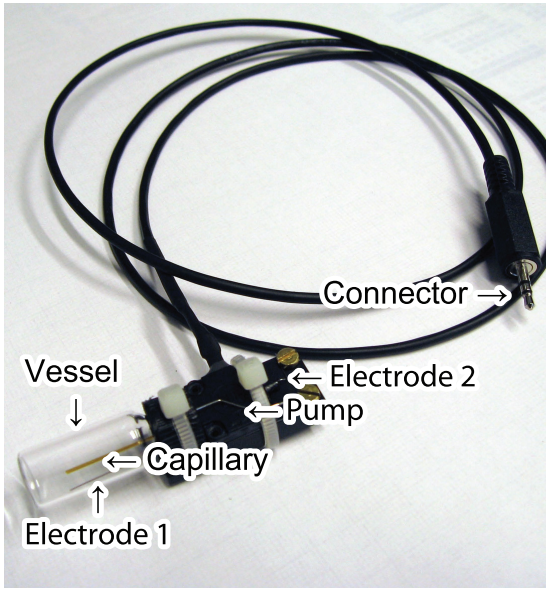

(a) The device

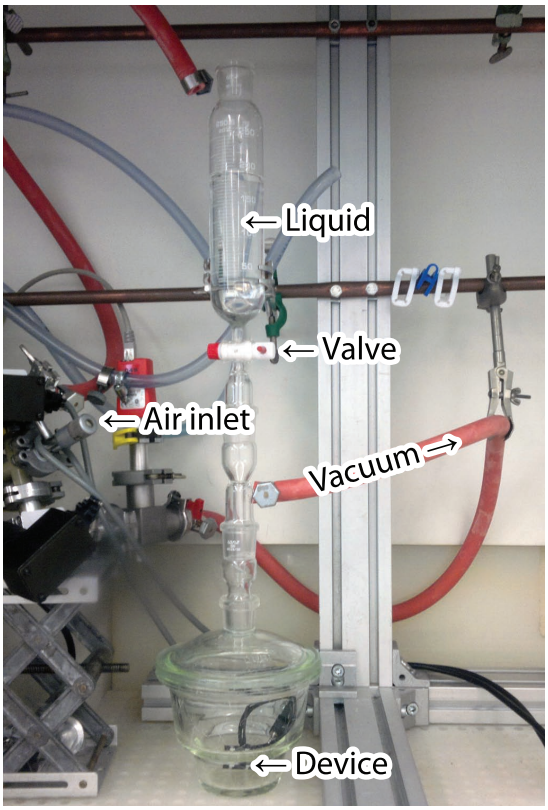

(b) The filling set up of the device

Figure 4.5.1: Two photogragraphs of the device and the filling setup

by the Hagen-Poiseuille equation[24]:

$$R_H = \frac{8\eta L}{\pi r^4} \text{ [kg/(s m}^4\text{)]} \tag{4.5.1}$$

Where η is the viscosity, L the length of the capillary and r the radius of the capillary. For air, water and VE this results in $R_H = 7.6 \times 10^{11}$, 4.2×10^{13} and 5.1×10^{15} Pa s/m^3.

During evacuation the pressure over the capillary becomes smaller and thus the evacuation of the device slows down ($\Delta P = P_0 e^{-t/\tau_{evac}}$ [Pa]). This is characterized by the hydraulic resistance and the hydrodynamic capacitance: C_H and is given by:

$$C_H = KV \text{ [m}^3\text{/Pa]} \tag{4.5.2}$$

where K [1/Pa] is the compressibility of the fluid and V [m^3] the volume of the container. The evacuation is of air, so $C_H = 1 \times 10^{-5}$ m^3/Pa, this results in a characteristic 'RC time,' $\tau_{evac} = R_H C_H$ of 0.21 s in air. So, for an reduction of air to 0.1% it takes $t = -\tau_{evac} \ln(\Delta P/P_0) = -0.21 \ln(0.001) = 1.5$ s.

4.5.2 Filling time

At first, since no pressure difference is present, the capillary will be filled by capillary action. Capillary action is caused by the decrease of surface energy. This force is transferred to pressure:

$$F_{surface} = C\sigma_s \cos\phi = 2\pi r \sigma_s \cos\phi \text{ [N]} \tag{4.5.3}$$

$$P_{surface} = \frac{F_{surface}}{A} = \frac{2\pi r \sigma_s \cos\phi}{\pi r^2} = \frac{2\sigma_s \cos\phi}{r} \text{ [Pa]} \tag{4.5.4}$$

Where σ_{st} [N/m] is the surface tension, ϕ [°] the contact angle and R [m] the radius of the capillary. So $P_{surface} = \frac{2\times72\times10^{-3}\cos(0)}{35\times10^{-6}} = 4.1\,\text{kPa} = 41\,\text{mbar}$, which is negligible compared to the 1 bar atmospheric pressure. To estimate the time it takes for the chip to fill, the hydraulic resistance of the capillary is calculated for water, while the hydraulic capacitance of air is assumed. This lead to a filling time of 82 s.

4.6 Expected experimental results

Using the parameters chapter 4 and an $\eta_0 = 0.50\,\text{Pa s}$ and a $t_m = 2\times10^{-3}\,\text{s}$ a plot is made of the expectations and shown in figure 4.6.1 and 4.6.1. It can be seen that the efficiency is below 0.4% which is quite low. The expected load current is around $200\,\text{nA}$ and the voltage $4\,\text{kV}$ at a frequency of $\omega_r \approx \frac{\pi}{2t_m\sqrt{\alpha}} = 640\,\text{krad/s} = 100\,\text{kHz}$ and an input power of $\frac{200\times10^{-9}4\times10^3}{4e-3} = 0.2$ W, which will not be feasible with the constructed device.

G_0/Pa	t_m/ s	η/ Pa s	α/–	ω/–
1.5×10^{1}	8.0×10^{-2}	1.2	1.3×10^{-5}	1.1×10^{4}
4.0×10^{1}	7.0×10^{-1}	2.8×10^{1}	6.3×10^{-8}	1.8×10^{4}
8.0×10^{1}	8.0×10^{-1}	6.4×10^{1}	2.4×10^{-8}	2.5×10^{4}
1.5×10^{2}	2.0×10^{-1}	3.0×10^{1}	2.0×10^{-7}	3.5×10^{4}
1.5×10^{2}	3.0×10^{-2}	4.5	9.1×10^{-6}	3.5×10^{4}
2.5×10^{2}	2.0×10^{-3}*	5.0×10^{-1}*	1.2×10^{-3}	4.5×10^{4}*
3.5×10^{2}	3.0×10^{-4}	1.1×10^{-1}	3.9×10^{-2}	5.3×10^{4}

Table 4.6.1: Measured relaxation times and viscosities by [31], α and ω are calculated with $H = 35\,\mu\text{m}$

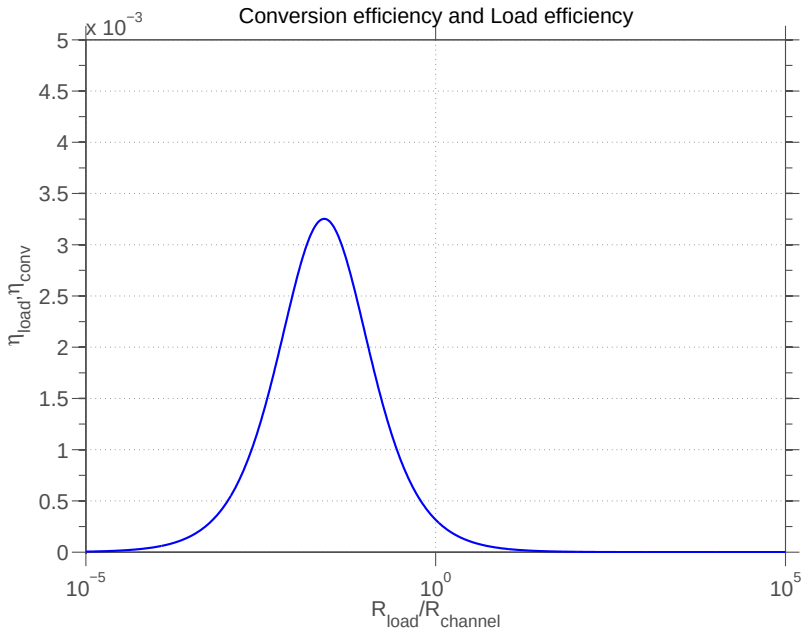

Figure 4.6.1: An estimation of the efficiency the experiments would achieve

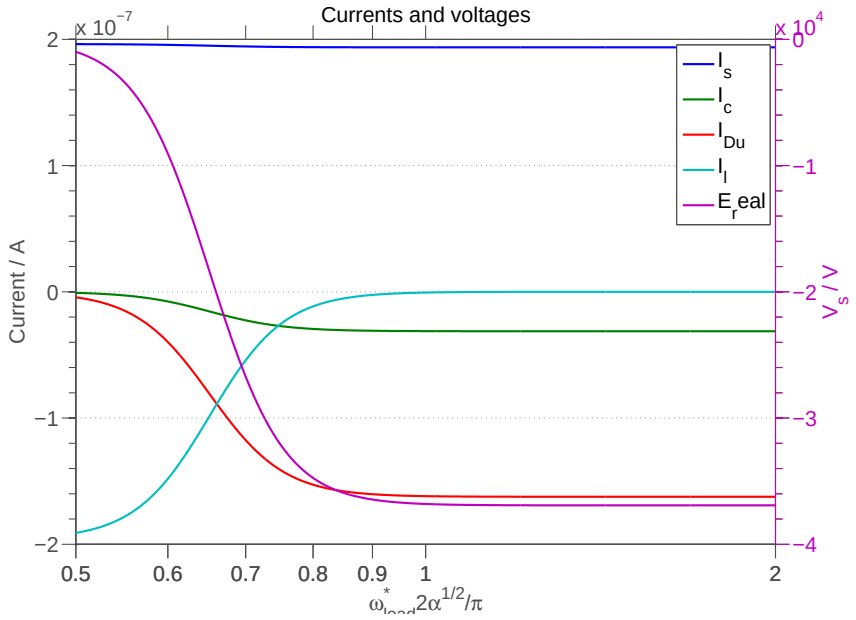

Figure 4.6.2: Expected currents and streaming voltage

5 Results

In the previous chapters a difference between my and Bandopadhyay's viewpoint became clear. In this chapter these differences will be discussed.

5.1 Electrical double layer simplification

To validate the simplified models, a numerical parameter sweep is done to compare the simple models (3.1.2) (ψ_2) and (3.1.3) (ψ_3) to the more extensive model proposed by Bandopadhyay (3.1.1) (ψ_1), the results are shown in table 5.1.1 and it can clearly be seen that $\bar{\psi}_3$ outperforms $\bar{\psi}_2$ in estimating $\bar{\psi}_1$, the results are also included graphically in figure 5.1.1.

Table 5.1.1: Potential parameter sweep, with $n = 1001$, $0 \leq \bar{y} \leq 1$ and $\varepsilon_{jk} = \frac{\sum_{i=1}^{n} |\psi_k(\bar{y}_i) - \psi_j(\bar{y}_i)|}{\sum_{i=1}^{n} |\psi_j(\bar{y}_i)|} \times 100\%$

$\bar{\zeta}$	$\bar{\lambda}$	$\varepsilon_{12}/\%$	$\varepsilon_{13}/\%$
-1	0.1	1.38	1.38
-5	0.1	31.9	31.9
-10	0.1	108	108
-1	0.5	12.9	1.28
-5	0.5	45.0	30.0
-10	0.5	127	104
-1	1	21.7	1.03
-5	1	51.0	25.3
-10	1	130.7	91.5

5.2 Reynolds number

The Reynolds number is calculated for the default parameters Bandopadhyay uses and is plotted in figure 5.2.1. It can be seen that the Reynolds number is far below 2300, so as expected an increase of mean velocity or height will need to be dramatically in order to create a turbulent flow.

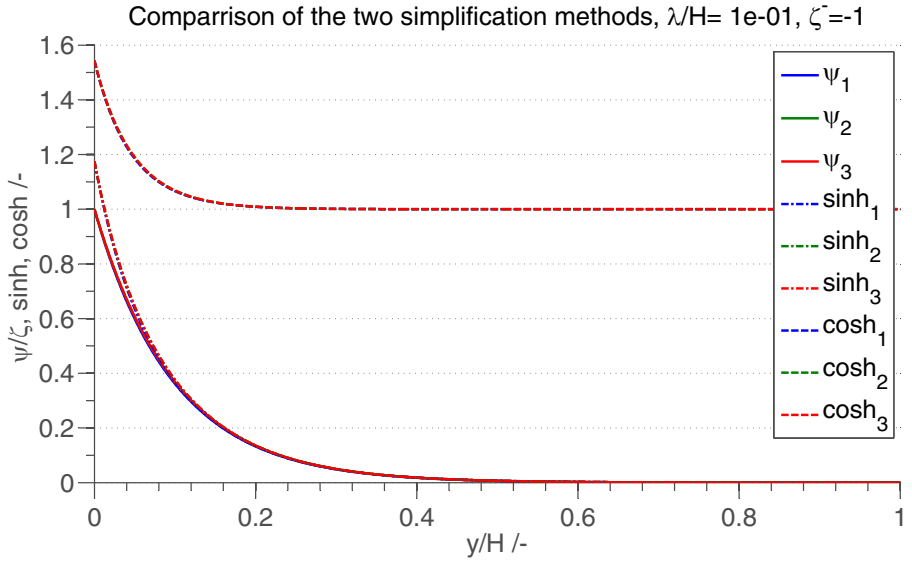

Figure 5.1.1: An illustration of the goodness of the simplification, with $\bar{\lambda} = 1/10$ and $\bar{\zeta} = -1$

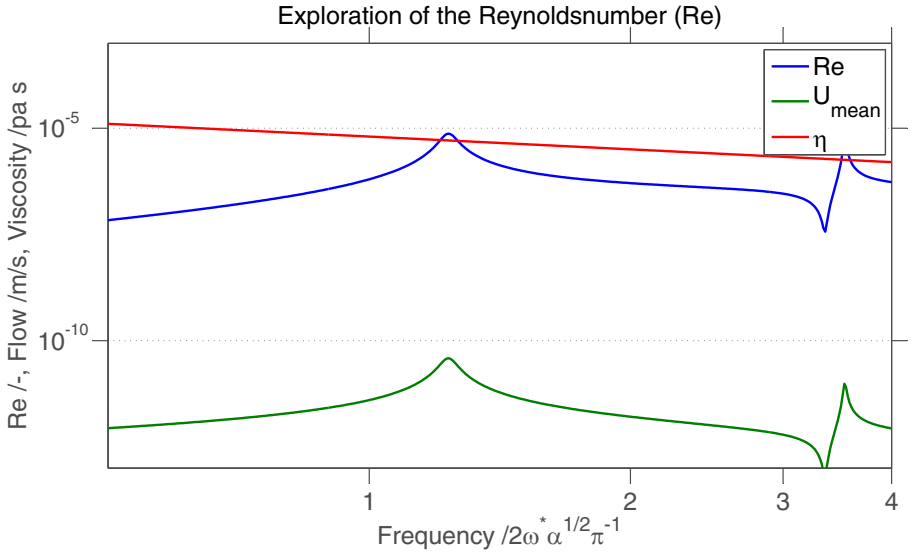

Figure 5.2.1: Reynolds number with $\eta_0 = 1 \times 10^{-2}$ Pa s, $t_m = 1e-3$, $\alpha = 1 \times 10^{-6}$, $J = -10$, $H = 100$ nm, $\lambda \equiv 1/10$

5.3 Efficiency

This thesis is all about energy conversion efficiency, which will be discussed in this final results section. First the simplifications made in the theory will be compared to Bandopadhyay's results, then the effects of the change of input power definition will be discussed and finally a load resistance will be added.

5.3.1 Simplification

The conversion efficiency of both the original model and the in section 3.1 proposed simplifications is shown in figure 5.3.1. It can be seen that the simplifications work well around the first resonance peak. However, in the second region they are less accurate for the lower α's, which makes sense since the neglected Ω and thus the Ω^2 terms become larger with increasing frequency and therefore are not negligible any more compared to 1. From now on only the first resonance peak is taken into consideration during the comparison.

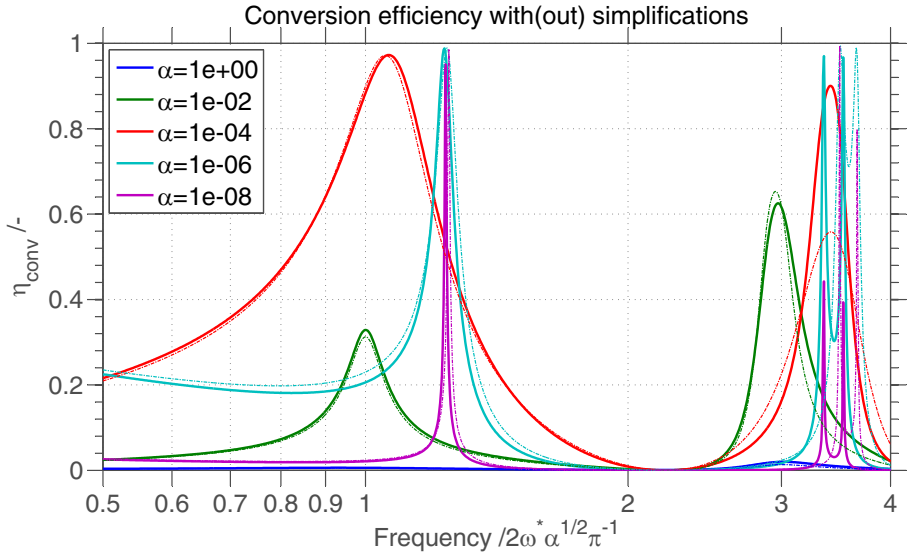

Figure 5.3.1: Comparison of the simplified conversion efficiency (solid lines) and Bandopadhyay's conversion efficiency (dashed lines) for different α's. Other parameters are: $\bar{\lambda} = 1/10$, $J = -10$, $Du = 0$.

5.3.2 Comparison between Bandopadhyay's and my theory

Some assumptions of Bandopadhyay need to have some extra nuances, which will be discussed in this section. First, the Dukhin number is checked, then the factor J is investigated and finally the consequences of the new definition of the input power is discussed.

Dukhin number

In (3.5.1) the minimum height of the channel to neglect the surface conduction current was defined as $H_{min} > 1 \times 10^{-7}/\sigma_b$ m, as the conductivity for Bandopadhyay's application is 0.67 S m[27] the minimum height has to be $H_{min} = 150$ nm, which is slightly bigger than the height he uses (100 nm) so the Dukhin number roughly negligible. However, red blood cells are responsible for the viscoelasticity of the blood[34] but are too big (≈ 1 µm to 10 µm[35]) to fit inside the channel, let alone to behave viscoelastic. So in order to make the proposed device work with blood, the dimensions should be reconsidered.

New input power definition

In figure 5.3.2 the calculated conversion efficiency is shown using the absolute flow as input power. As was expected, the efficiency has dropped using the new definition for input power. Except for the peak with the low α.

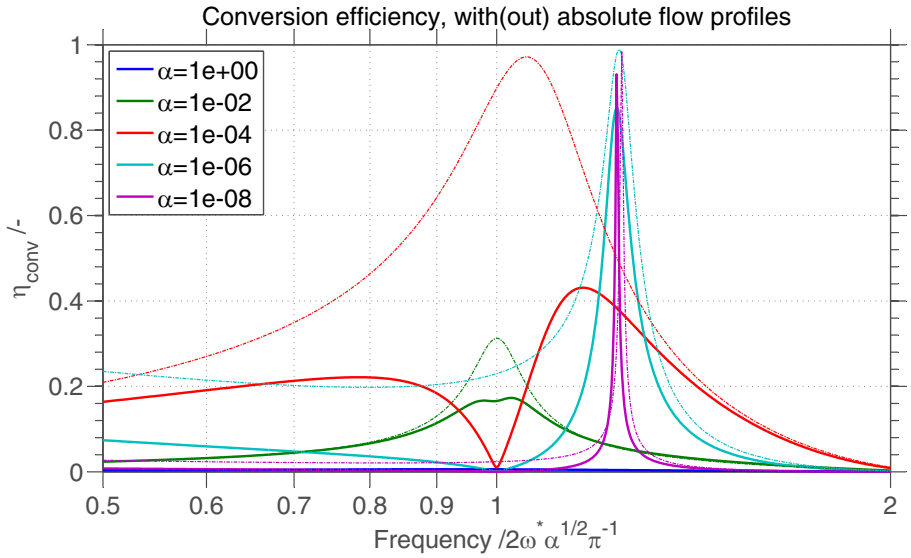

Figure 5.3.2: The resulting graphs after changing the definition of input power (solid) and the simplified conversion efficiency defined by Bandopadhyay. $\bar{\lambda} = 1/10$, $J = -10$, $Du = 0$

Dependency of J on the viscosity and the frequency

The estimated efficiencies of α and J proposed in table 3.4.1 are shown in figure 5.3.3. As can be seen in all cases, if $\alpha = 1$ the conversion efficiency is not noticeable.

Figure 5.3.3a shows comparable peaks as Bandopadhyay's theory, however the resonance frequency has shifted more towards $2t_m\sqrt{\alpha}/\pi$ and the peaks become narrower. Which both can be explained by the increase in J and therefore an increase in the frequency where the real part of the numerator of (3.6.1) becomes higher.

The frequency dependent J factor introduces an extra shift in resonance frequency and widens the peaks. It seems that an α of 1×10^{-2} would be optimal, however this would mean a resonance frequency of $\omega_r \approx \frac{\pi}{2t_m\sqrt{\alpha}} = 16\,\text{Mrad/s} \rightarrow f_r = 2.5\,\text{MHz}$. Which is, in my opinion, not feasible.

In figure 5.3.3c and 5.3.3d the input power is defined as the integral of the absolute value of the flow profile times the pressure. It can be seen that the maximum efficiency is roughly cut in half and the resonance peaks now have become minima.

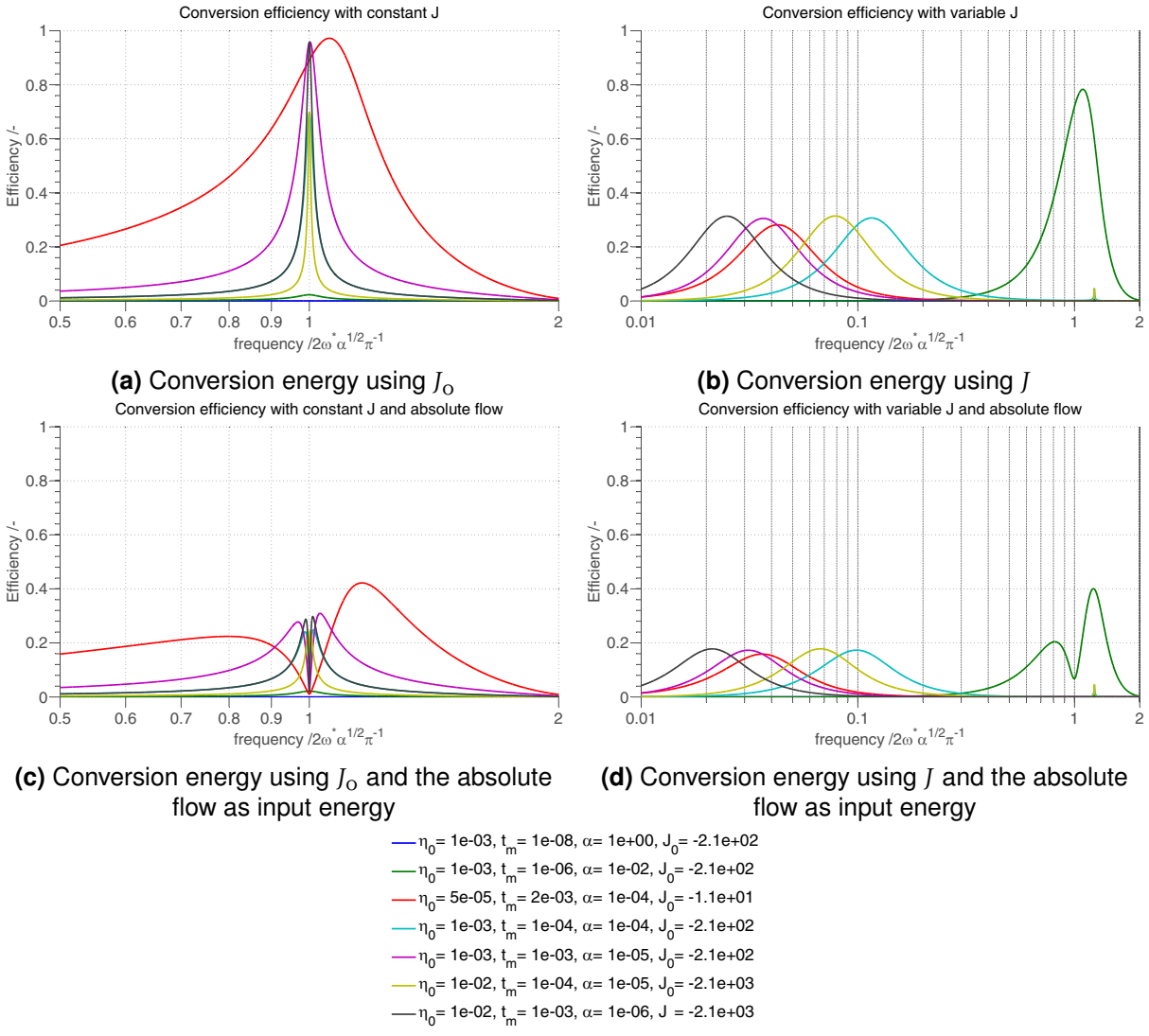

(a) Conversion energy using J_0

(b) Conversion energy using J

(c) Conversion energy using J_0 and the absolute flow as input energy

(d) Conversion energy using J and the absolute flow as input energy

Figure 5.3.3: Four graphs showing the impact of the new definitions of J and the new definition of the input power. $\bar{\lambda} = 1/10$ and $Du = 0$.

5.3.3 Load resistance

A load resistor sweep is made in five different conditions: $J = -10$, $J = J_0$ with(out) an absolute flow, $J = J(\omega^*)$ with(out) an absolute flow. It is expected that the load efficiency is half the conversion efficiency if the load resistivity is equal to the internal resistivity of the channel. In figure 5.3.4 plots are made of both the conversion efficiency (independent of the load resistance, dashed line) and the load efficiency as function of the load resistivity ($\rho_{load} = R_{load}A/m$ [Ω m]) normalized by the channel resistivity ($\rho_{channel} = 1/\sigma_b$ [Ω m]). As well as the frequency at which the highest efficiency is expected.

In figure 5.3.4a it can be seen that if Bandopadhyay's model is used, two plots (red and cyan) are obscured since another plot with the same value of α is present. Also, the maximum load efficiency is near the maximum of the conversion efficiency. In figure 5.3.4b the frequency shifts towards a higher plateau at the point that the resistivity of the load is equal to the resistivity of the channel. This plateau is equal to the frequency at which an unloaded device works. Which is as expected, since a a high load resistance will not influence the device as it behaves as an open terminal.

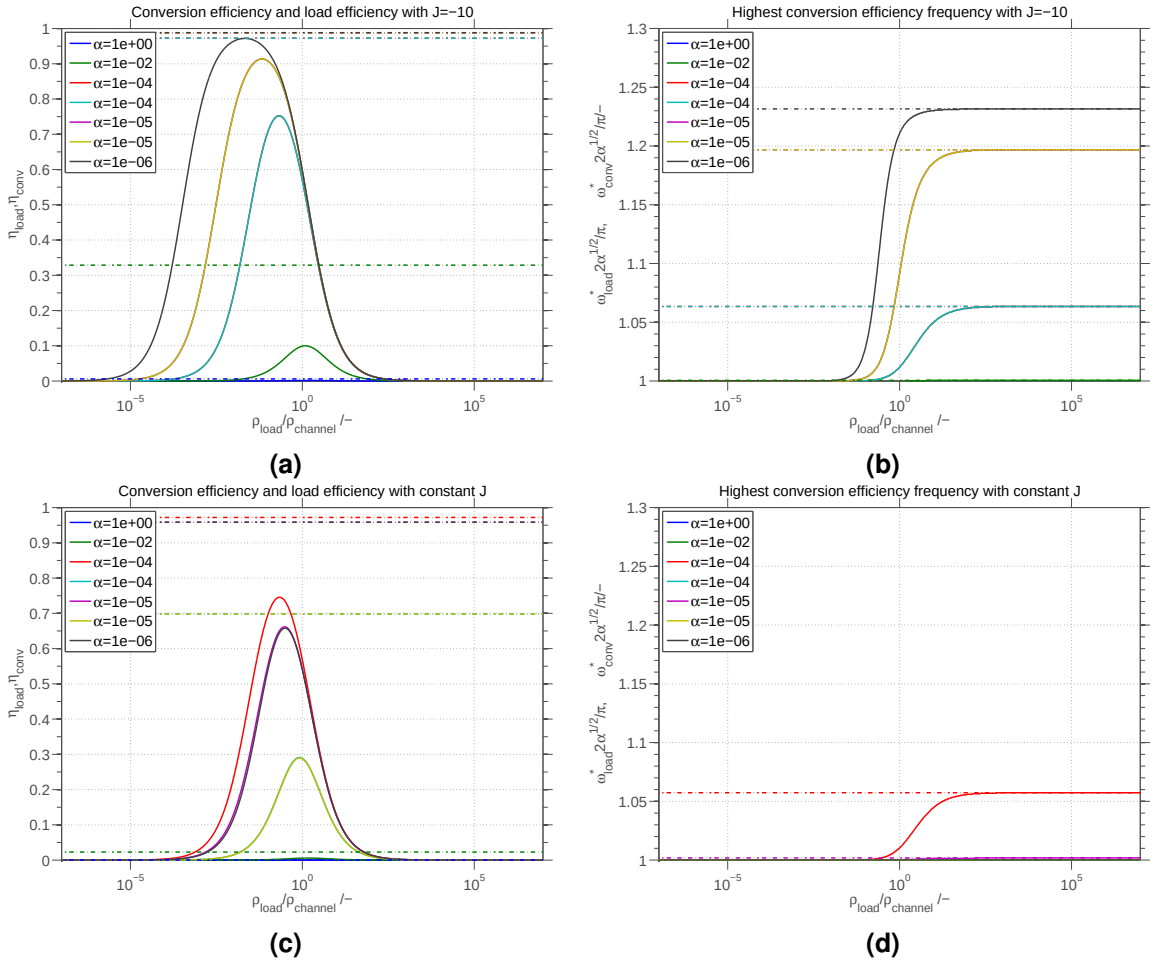

Figure 5.3.4: The efficiency and optimum frequency as a function of $\rho_{load}/\rho_{channel}$ with parameters $\bar{\lambda} = 1/10$ and $Du = 0$

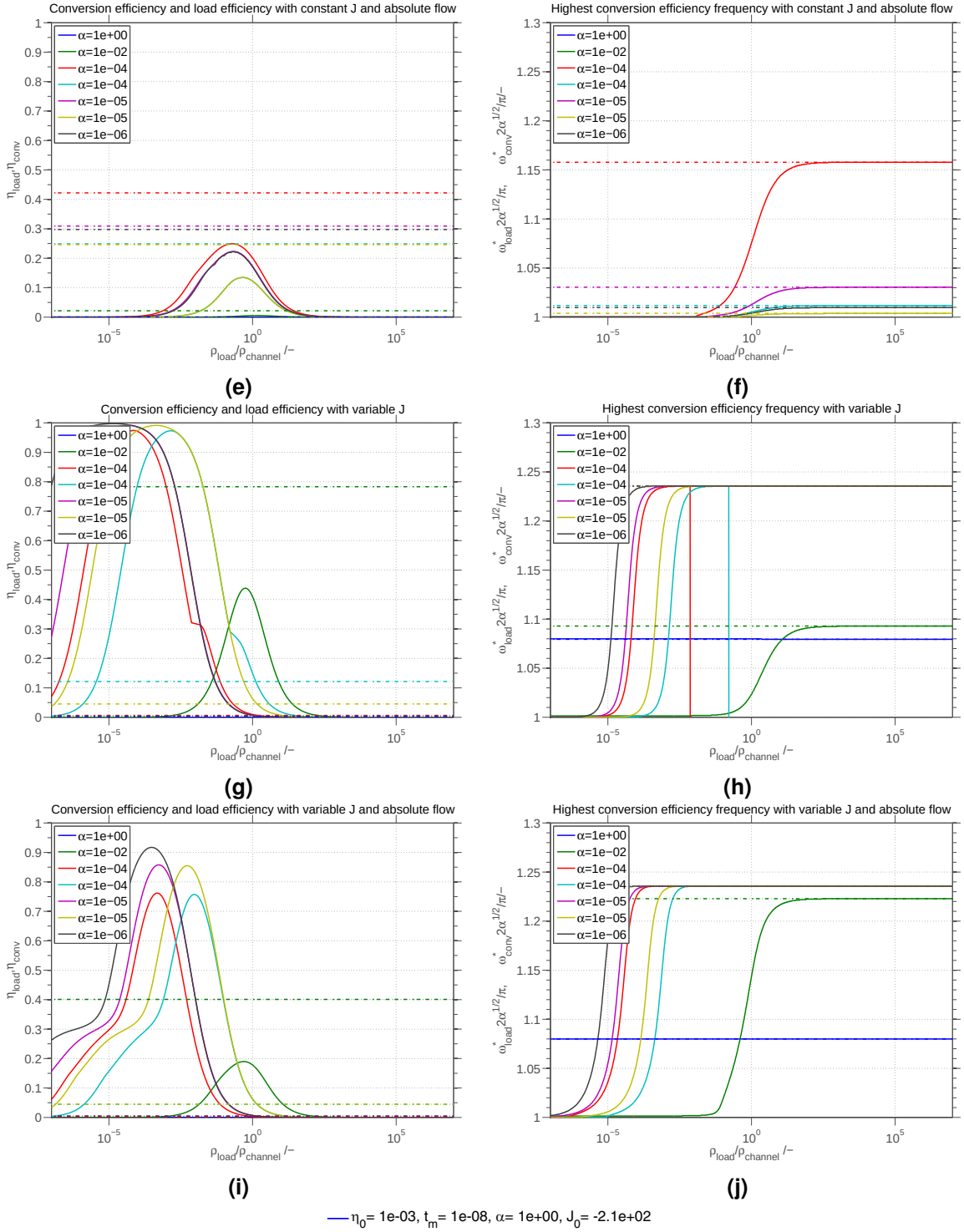

Figure 5.3.4: Continued. The efficiency and optimum frequency as a function of $\rho_{load}/\rho_{channel}$ with parameters $\bar{\lambda} = 1/10$ and $Du = 0$

Figure 5.3.4c on the next row has different J parameters as is explained in section 3.4. The only system that does not change, compared to figure 5.3.4a is the red line, since it still has $J = -10$, all other lines have decreased a lot. The normalized frequency for maximum efficiency has become closer to 1, as can be seen in figure 5.3.4d. Which is in agreement with figure 5.3.3a.

The results of changing the definition of input power with constant J's are plotted in figure 5.3.4e. It can be seen that the load efficiency has decreased, as is expected. The frequencies in 5.3.4f deviate more from the normalized frequency if J decreases.

In figure 5.3.3g and 5.3.3i the bell shaped plots have changed appearance. Probably this is due to the extra frequency dependence introduced by the frequency dependent J. This can also be seen in the frequency plots in figures 5.3.3h and 5.3.3j.

For now it is difficult to say what system is correct, but I would say the system with constant J and absolute flow (figure 5.3.4e). The maximum achievable conversion efficiency using Bandopadhyay's parameters is 31% (purple), since the red line is not considered by Bandopadhyay. This would lead to an operating frequency of $\omega_r \approx \frac{\pi}{2t_m\sqrt{\alpha}} = 0.50\,\text{Mrad/s} = 80\,\text{kHz}$.

6 Conclusions

In this chapter the goals of this project are compared to the results which are obtained.

6.1 Findings

The goal of this project was to see if the predictions Bandopadhyay made are feasible and to understand and verify his theories. The theories are re-investigated and the results appeared to be overestimated, due to assumptions which could be to simplistic. Not only because the theory only holds for the conversion from hydraulic to electric power and not for the harvesting of power, but also because of the fact that the predictions were overestimated, because of a poorly defined input power.

During this project the complexity of not only the mathematics, but especially the physical meaning became clear. After seven months of investigation; looking for similar papers and experiments; and thinking of comparable systems it still is partly obscured. The models of Bandopadhyay are explored, torn apart and put together again to find a more realistic model.

Because of the dependence of all parameters it is hard to create a framework which will provide a short list of design rules. All changes in the parameters for Bandopadhyay's model resulted in lower conversion efficiencies, so I think the proposed system is the optimized version and can not be optimized further.

The found conversion efficiency for the proposed system by Bandopadhyay is found to be 31%, the maximum load efficiency for the same system is 22% at $80\,\mathrm{kHz}$. Which is in big contrast with the claimed conversion efficiency of 98% and subsequently an load efficiency of 96%.

An experimental set up has been designed and constructed, however because of a deficient planning and a broken pump no measurements were conducted. Probably the designed set up would not have worked, since the frequencies needed for the available viscoelastic fluid are to high for the small pump. Also, the viscosity of the liquid is probably to high for the small capillaries.

Therefore the theoretical paper which had to be converted into a practical paper is now analysed thoroughly and the bright prospects are tampered.

6.2 Limitations

Since the theoretical work is based on the Maxwell model, which is only valid for low shear rates, the efficiencies might not be as high as expected since the model is not valid any more. Also, the theoretical work is created for rectangular channels, whereas the device is made of a round capillary. This could influence the calculations, but probably in a positive way since the surface/volume ratio is higher.

6.3 Future work

This project can be prolonged by trying to find the physical phenomena which take part in the system and create a physical picture of it. This can be done by someone in the field of physics of fluids and has more experience with viscoelasticity. The equations can be mastered with time, but a gut feeling about what happens physically will take hands on experience on macro, micro and probably even nanoscale. [1]

A Buckingham-π analysis can also give more insight in the subject and possibly reduce the complexity and the number of parameters. However, since everything is already normalized I guess it is already be done by Bandopadhyay.

[1] In order to get more insight in the flow profiles, one should look at Casanellas paper[36], which I found during my research but did not understand, on the final day of my thesis I re-found it and I think it is very useful for understanding.

Bibliography

[1] J. W. McBain, “The Conception and Properties of the Electrical Double Layer and its Relation to Ionic Migration,” *The Journal of Physical Chemistry*, vol. 99, no. 1913, 1924.

[2] H. Mizutani, T. Ishido, T. Yokokura, and S. Ohnishi, “Electrokinetic phenomena associated with earthquakes,” *Geophysical Research Letters*, vol. 3, no. 7, 1976.

[3] F. D. Morgan, E. R. Williams, and T. R. Madden, “Streaming potential properties of westerly granite with applications,” *Journal of Geophysical Research*, vol. 94, no. B9, p. 12449, 1989.

[4] L. Jouniaux and J. Pozzi, “Streaming potential and permeability of saturated sandstones under triaxial stress: Consequences for electrotelluric anomalies prior to earthquakes,” *Journal of Geophysical Research*, 1995.

[5] A. Revil and A. Jardani, “Seismoelectric response of heavy oil reservoirs: theory and numerical modelling,” *Geophysical Journal International*, vol. 180, pp. 781–797, Feb. 2010.

[6] F. H. J. van der Heyden, D. J. Bonthuis, D. Stein, C. Meyer, and C. Dekker, “Electrokinetic energy conversion efficiency in nanofluidic channels.,” *Nano letters*, vol. 6, pp. 2232–7, Oct. 2006.

[7] P. Goswami and S. Chakraborty, “Energy transfer through streaming effects in time-periodic pressure-driven nanochannel flows with interfacial slip.,” *Langmuir : the ACS journal of surfaces and colloids*, vol. 26, pp. 581–90, Jan. 2010.

[8] J. N. Groves and A. R. Sears, “Alternating streaming current measurements,” *Journal of Colloid and Interface Science*, vol. 53, pp. 83–89, Oct. 1975.

[9] P. M. Reppert, F. D. Morgan, D. P. Lesmes, and L. Jouniaux, “Frequency-Dependent Streaming Potentials.,” *Journal of colloid and interface science*, vol. 234, pp. 194–203, Feb. 2001.

[10] A. Bandopadhyay and S. Chakraborty, “Giant augmentations in electro-hydro-dynamic energy conversion efficiencies of nanofluidic devices using viscoelastic fluids,” *Applied Physics Letters*, vol. 101, no. 4, p. 043905, 2012.

[11] P. Scales, F. Grieser, T. Healy, L. White, and D. Chan, “Electrokinetics of the silica-solution interface: a flat plate streaming potential study,” *Langmuir*, no. 10, pp. 965–974, 1992.

[12] H. L. F. v. Helmholtz, "Studies of electric boundary layers," *Annals Physik Wiedemann, Leipzig*, pp. 337–382, 1879.

[13] R. J. Hunter, *Zeta Potential in Colloid Science: Principles and Applications*. Colloid science, Academic Press, 1981.

[14] F. a. Morrison and J. F. Osterle, "Electrokinetic Energy Conversion in Ultrafine Capillaries," *The Journal of Chemical Physics*, vol. 43, no. 6, p. 2111, 1965.

[15] B. Kirby, *Micro- and Nanoscale Fluid Mechanics: Transport in Microfluidic Devices*. Cambridge University Press, 2013.

[16] D. Gillespie, "High energy conversion efficiency in nanofluidic channels.," *Nano letters*, vol. 12, pp. 1410–6, Mar. 2012.

[17] W. M. Haynes, T. J. Bruno, and R. L. David, *CRC Handbook of Chemistry and Physics*. Internet Version, 2014.

[18] E. Miller, "The dynamics and rheology of shear-banding wormlike micelles and other non-newtonian fluids," Tech. Rep. May, University of Massachusetts Amherst, 2007.

[19] S. C. Sharma, L. K. Shrestha, K. Tsuchiya, K. Sakai, H. Sakai, and M. Abe, "Viscoelastic wormlike micelles of long polyoxyethylene chain phytosterol with lipophilic nonionic surfactant in aqueous solution.," *The journal of physical chemistry. B*, vol. 113, pp. 3043–50, Mar. 2009.

[20] M. Buchanan, M. Atakhorrami, J. Palierne, F. MacKintosh, and C. Schmidt, "High-frequency microrheology of wormlike micelles," *Physical Review E*, vol. 72, p. 011504, July 2005.

[21] A. Bandopadhyay and S. Chakraborty, "Electrokinetically induced alterations in dynamic response of viscoelastic fluids in narrow confinements," *Physical Review E*, vol. 85, p. 056302, May 2012.

[22] J. H. Masliyah and S. Bhattacharjee, *Electrokinetic and colloid transport phenomena*. Wiley interscience, 2006.

[23] A. A. Lambert, S. Cuevas, J. A. del Río, and M. López de Haro, "Heat transfer enhancement in oscillatory flows of Newtonian and viscoelastic fluids," *International Journal of Heat and Mass Transfer*, vol. 52, pp. 5472–5478, Nov. 2009.

[24] R. Byron Bird, W. E. Stewart, and E. N. Lightfoot, *Transport phenomena*. John Wiley & Sons, New York, 2002.

[25] J. M. Dealy, "Weissenberg and deborah numbers - their definition and use," *Rheol. Bull*, vol. 79, no. 2, pp. 14–18, 2010.

[26] D. Roylance, "Engineering viscoelasticity," tech. rep., Department of Materials Science and Engineering - Massachusetts Institute of Technology, 2001.

[27] K. L. K. Costeloe, D. W. Hill, and S. N. Mohapatra, "Blood resistivity and its implications for the calculation of cardiac output by the thoracic electrical impedance technique," *Intensive care medicine*, vol. 67, pp. 63–67, 1977.

[28] C. Werner, H. Körber, R. Zimmermann, S. Dukhin, and H. J. H. Jacobasch, "Extended Electrokinetic Characterization of Flat Solid Surfaces.," *Journal of colloid and interface science*, vol. 208, pp. 329–346, Dec. 1998.

[29] J. Lyklema and M. Minor, "On surface conduction and its role in electrokinetics," *Colloids and Surfaces A: Physicochemical and Engineering Aspects*, vol. 140, pp. 33–41, Sept. 1998.

[30] A. Crespy, A. Bolève, and A. Revil, "Influence of the Dukhin and Reynolds numbers on the apparent zeta potential of granular porous media.," *Journal of colloid and interface science*, vol. 305, pp. 188–94, Jan. 2007.

[31] A. Maestro and D. P. Acharya, "Formation and disruption of viscoelastic wormlike micellar networks in the mixed surfactant systems of sucrose alkanoate and polyoxyethylene alkyl ether," *The Journal of . . .*, pp. 14009–14016, 2004.

[32] C. A. Dreiss, "Wormlike micelles: where do we stand? Recent developments, linear rheology and scattering techniques," *Soft Matter*, vol. 3, no. 8, p. 956, 2007.

[33] R. M. Pashley, M. Rzechowicz, L. R. Pashley, and M. J. Francis, "De-gassed water is a better cleaning agent.," *The journal of physical chemistry. B*, vol. 109, pp. 1231–8, Jan. 2005.

[34] J. A. del Río, M. López de Haro, and S. Whitaker, "Enhancement in the dynamic response of a viscoelastic fluid flowing in a tube," *Physical Review E*, vol. 58, pp. 6323–6327, Nov. 1998.

[35] T. R. Gregory, "The bigger the C-value, the larger the cell: genome size and red blood cell size in vertebrates.," *Blood cells, molecules & diseases*, vol. 27, no. 5, pp. 830–43, 2001.

[36] L. Casanellas and J. Ortín, "Laminar oscillatory flow of Maxwell and Oldroyd-B fluids: Theoretical analysis," *Journal of Non-Newtonian Fluid Mechanics*, vol. 166, pp. 1315–1326, Dec. 2011.

[37] S. Chakraborty and S. Das, “Streaming-field-induced convective transport and its influence on the electroviscous effects in narrow fluidic confinement beyond the Debye-Hückel limit,” *Physical Review E*, vol. 77, p. 037303, Mar. 2008.

A Abbreviations, Definitions and Symbols

A.1 Abbreviations

EDL Electrical Double Layer

EOF Electro Osmotic Flow

PDF Pressure Driven Flow

A.2 Definitions

Deborah number The Deborah number is intended to describe the extend to which the response of a material to a deformation is viscoelastic rather than purely viscous[25].

Debye length In the Debye-HÃijckel theory of ionic solutions, the effective thickness of the cloud of ions of opposite chargewhich surrounds each given ion and shields the Coulomb potentialproduced by that ion[17].

Reynolds number A dimensionless quantity used in fluid mechanics, defined by $Re = \rho u L/\eta$, where ρ is density, u is velocity, L is length, and η is viscosity[17].

ζ **potential** The electric potential at the surface of a colloidal particle relative to the potential in the bulk medium at a long distance. Also called electrokinetic potential[17].

A.3 Dimensional symbols

C_{norm} Normalization constant $J \frac{\epsilon\zeta}{\frac{dp}{dx}H^2}\frac{1}{\sigma_b}$[m²/A]

e Electron charge $[1.6 \times 10^{-19}\,\mathrm{C}]$

E_s Streaming potential field [V/m]

ϵ permittivity of the fluid [F/m]

H Channel half height [m]

I_c Bulk conduction current density [A/m²]

I_{Du} Stern-layer conduction current density [A/m²]

I_s Streaming current density[A/m²]

λ Debye length [m]

k_B Boltzman constant $[1.4 \times 10^{-23}\,\mathrm{J/K}]$

$n_{\pm}$ Ionic number [1/m³]

n_0 Bulk ionic concentration [1/m³]

ω Frequency [rad/s]

dp/dx Pulsating pressure gradient amplitude [Pa/s]

ψ Electrical potential distribution within the EDL [V]

Q Volumetric flow density [m³/s]

u Velocity field [m/s]

U Fourier transformed velocity field [m/s]

ρ_e Volumetric charge density [C/m³]

σ_b Bulk conductivity [S/m]

σ_{st} Stern-layer conductivity [S/m²]

T Absolute temperature [K]

t_m Relaxation time [s]

V_T Thermal voltage $\frac{k_B T}{e} = 25\,\mathrm{mV}$

y Distance from the wall [m]

ζ Zeta potential [V]

z Valence [–]

A.4 Non dimensional and dimensionless symbols

α Inverse Deborah number $\frac{\rho H^2}{\eta t_m}[-]$

$\bar{E}_s$ Non-dimensional streaming potential [–]

J Reference current ratio [–]

$\bar{\lambda}$ Non-dimensional Debye length $\frac{\lambda}{H}[-]$

η_{eff} Conversion efficiency [–]

ω^* Non-dimensional frequency: $\omega t_m[-]$

U^* Non-dimensional velocity field $U\frac{\eta}{\partial P/\partial x H^2}[-]$

$\bar{\psi}$ Non-dimensional electrical potential distribution: $\psi/\zeta[-]$

$\bar{y}$ Non-dimensional distance from the wall $\frac{y}{H}[-]$

$\bar{\zeta}$ Non-dimensional Zeta potential: $\frac{ze\zeta}{k_B\tilde{T}} = \frac{z\zeta}{V_T}[-]$

B Derivation of equations

B.1 Calculation of the streaming potential

This section elaborates upon the calculation of the electrical field by Bandopadhyay and Chakraborty[10], it starts with Kirchhoff's current law:

$$A(I_s + I_c + I_{Du}) = 0 \text{ [A]} \tag{B.1.1}$$

The current relations (2.3.5), (2.3.9) and (2.3.10) are plugged into equation (B.1.1):

$$2zen_0 \int_0^H \sinh\left(\frac{z}{V_T}\psi(y)\right) U(y,\omega)dy + E_s(\omega)\sigma_b \int_0^H \cosh\left(\frac{z}{V_T}\psi(y)\right)dy + E_s(\omega)\sigma_b Du = 0 \text{ [A/m}^2\text{]} \tag{B.1.2}$$

This equation is multiplied by the normalization constant:

$$C_{norm} = \frac{\eta k_B T}{2\frac{dp}{dx}H^2 n_0 \zeta z^2 e^2} = J\frac{\epsilon\zeta}{\frac{dp}{dx}H^2}\frac{1}{\sigma_b} \text{ [m}^2\text{/A]} \tag{B.1.3}$$

, with J [–] the fraction of reference streaming current ($I_{c,ref}$ [A]) versus reference conduction current ($I_{s,ref}$ [A]):

$$J = \frac{I_{c,ref}}{I_{s,ref}} = \frac{A2z^2e^2E_{ref}n_0/f}{-2Az^2e^2n_0U_{ref}\zeta/k_BT} = \frac{2z^2e^2U_{ref}\eta n_0\sigma_b/2n_0z^2e^2\epsilon\zeta}{-2z^2e^2n_0U_{ref}\zeta/k_BT} = -\frac{\sigma_b\eta\lambda^2}{\epsilon^2\zeta^2} \text{ [–]} \tag{B.1.4}$$

where U_{ref} [m/s] is the reference velocity field, $E_{ref} = U_{ref}\eta/\epsilon\zeta$ [V/m] the reference voltage field and $f = 2n_0e^2z^2/\sigma_b$ [kg/s] the ionic friction factor , (B.1.2) then becomes:

$$\int_0^H \frac{U(y,\omega)\eta}{\frac{dp}{dx}H^2}\frac{k_BT}{\zeta ze}\sinh\left(\frac{z}{V_T}\psi(y)\right)dy + J\frac{E_s(\omega)\epsilon\zeta}{\frac{dp}{dx}H^2}\int_0^H \cosh\left(\frac{z}{V_T}\psi(y)\right)dy + JDu\frac{E_s(\omega)\epsilon\zeta}{\frac{dp}{dx}H^2} = 0 \text{ [–]} \tag{B.1.5}$$

Using the known normalization parameters it is then nondimensionalized into:

$$\int_0^1 U^*(\bar{y},\omega)\frac{\sinh(\bar{\zeta}\bar{\psi}(\bar{y}))}{\bar{\zeta}}d\bar{y} + J\bar{E}_s(\omega)\int_0^1 \cosh(\bar{\zeta}\bar{\psi}(\bar{y}))d\bar{y} + JDu\bar{E}_s(\omega) = 0 \text{ [–]} \tag{B.1.6}$$

$U^*(\bar{y},\omega)$ consists of two parts: one is independent of the streaming potential (the pressure driven flow part, $U_p^*(\bar{y},\omega)$) and one part is dependent of the streaming potential (the electroviscous part, $U_{E_s}^*(\bar{y},\omega) = \bar{E}_s(\omega)U_{E_s}^{**}(\bar{y},\omega)$) [37]. Splitting these two parts results the following relation with four terms:

$$\int_0^1 U_p^*(\bar{y},\omega)\frac{\sinh(\bar{\zeta}\bar{\psi}(\bar{y}))}{\bar{\zeta}}d\bar{y} + \bar{E}_s(\omega)\int_0^1 U_{E_s}^{**}(\bar{y},\omega)\frac{\sinh(\bar{\zeta}\bar{\psi}(\bar{y}))}{\bar{\zeta}}d\bar{y} + J\bar{E}_s(\omega)\int_0^1 \cosh(\bar{\zeta}\bar{\psi}(\bar{y}))d\bar{y} + JDu\bar{E}_s(\omega) = 0\ [-] \tag{B.1.7}$$

Which is simplified into:

$$\iota_1 + \bar{E}_s\iota_2 + J\iota_3\bar{E}_s + JDu\bar{E}_s = 0\ [-] \tag{B.1.8}$$

where $\iota_1 = \int_0^1 U_p^*(\bar{y},\omega)\frac{\sinh(\bar{\zeta}\bar{\psi}(\bar{y}))}{\bar{\zeta}}d\bar{y}$, $\iota_2 = \int_0^1 U_{E_s}^{**}(\bar{y},\omega)\frac{\sinh(\bar{\zeta}\bar{\psi}(\bar{y}))}{\bar{\zeta}}d\bar{y}$ and $\iota_3 = \int_0^1 \cosh(\bar{\zeta}\bar{\psi}(\bar{y}))d\bar{y}$, to obtain the streaming potential, it is rearranged to:

$$\bar{E}_s = \frac{-\iota_1}{\iota_2 + J(\iota_3 + Du)}\ [-] \tag{B.1.9}$$

C Jacobi's law

C.1 Maximum power transfer

The current through the load is:

$$I_l = V_s/R_l \text{ [A]} \tag{C.1.1}$$

and the voltage over the load is:

$$V_l = I_s \frac{R_c R_l}{R_c + R_l} \text{ [V]} \tag{C.1.2}$$

The load power is can then be calculated as:

$$P_l = I_l V_s = V^2/R_l = I_s^2 \left(\frac{R_c R_l}{R_l + R_c} \right)^2 / R_l = \frac{R_c^2}{R_c^2/R_l + 2R_c + R_l} \text{ [W]} \tag{C.1.3}$$

Which is maximum if $R_l = R_c$, so at that point the maximum power transfer is available.

C.2 Maximum power transfer efficiency

The maximum power transfer efficiency is defined as:

$$\eta_p = \frac{P_l}{P_{tot}} = \frac{P_l}{P_c + P_l} = \frac{V_s^2/R_l}{V_s^2/R_l + V_s^2/R_c} = \frac{R_c}{R_l + R_c} \text{ [–]} \tag{C.2.1}$$

which is maximum if $R_l >> R_c$.

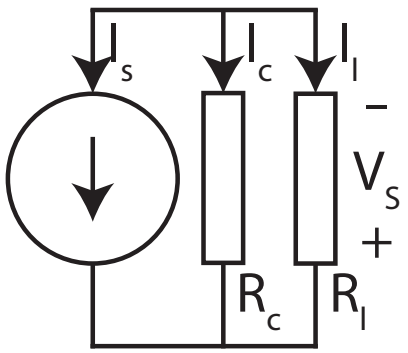

Figure C.1.1: The electrical model of the system

D Matlab functions

In this chapter the used MATLAB functions are presented.

D.1 Bandopadhyay model

```
function [I1,I2,I3,EsBar,Q,psi,sqrtAlphaOmega_]=BandopadhyayModelFreq(omega,alpha,
    lambdaBar,zeta,J,Du,dy)
% omega=omega*
% omega_=omegaBar
y=0:dy:1;
omega_=1i*omega+omega.^2;

% start calculations
psi=cosh((y-1)/(lambdaBar))/cosh(1/lambdaBar);
% psi=exp(-y/lambdaBar);
I1=zeros(size(omega));
I2=zeros(size(omega));
I3=zeros(size(omega));
C1=(1-1i*omega)./(alpha*omega_);
C2=(1-1i*omega)./(1+alpha*omega_*(lambdaBar)^2);
sqrtAlphaOmega_=sqrt(alpha*omega_);
cosSqrtAlphaOmega_=cos(sqrtAlphaOmega_);
parfor i=1:length(y)
    dI1=C1.*(1-(cos(sqrtAlphaOmega_*(1-y(i)))./cosSqrtAlphaOmega_)*psi(i);
    I1=I1+dI1*dy;
    dI2=C2.*(psi(i)-(cos(sqrtAlphaOmega_*(y(i)-1)))./cosSqrtAlphaOmega_)*psi(i);
    I2=I2+dI2*dy;
    dI3=cosh(zeta*psi(i));
    I3=I3+dI3*dy;
end
EsBar=-I1./(I2+J*(I3+Du));

Q=zeros(size(omega));
for i=1:length(y)
    dQpdf=C1.*(1-(cos(sqrtAlphaOmega_*(1-y(i)))./cosSqrtAlphaOmega_);
    dQeof=EsBar.*C2.*(psi(i)-(cos(sqrtAlphaOmega_*(y(i)-1)))./cosSqrtAlphaOmega_);
    dQ=dQpdf+dQeof;
    Q=Q+dQ*dy;
end
end
```

D.2 Simplified Bandopadhyay model

```
function[I1,I2,I3,E,Q,Omega]= BandopadhyayModelFreqSimple(omega,alpha,lambdaBar,J,Du,I4)
narginchk(4,6)
if nargin==4
    Du=0;
end
if nargin==5
    I4=0;
end
Omega=sqrt(alpha*(1i*omega+omega.^2));
I1=lambdaBar*(1-1i*omega).*(lambdaBar^2-lambdaBar.*tanc(Omega));
I2=-lambdaBar*(1-1i*omega).*(1/2+lambdaBar*Omega.*tan(Omega));
I3=1*ones(size(omega));
E=-I1./(I2+J.*(I3+Du+I4));
Q=(1-1i*omega)./Omega.^2.*(1-tanc(Omega))...
    +E.*(1-1i*omega).*(lambdaBar-tanc(Omega));
end
```

D.3 Bandopadhyay model with absolute flow

```
function [I1,I2,I3,EsBar,Q,psi,Omega]=BandopadhyayModelFreqQabs(omega,alpha,lambdaBar,zeta
    ,J,Du,dy,I4)
% omega=omega*
% omega_=omegaBar
narginchk(2,8);
if nargin<3
    lambdaBar=0.1;
end
if nargin<4
    zeta=25e-3;
end
if nargin<5
    J=-10;
end
if nargin<6
    Du=0;
end
if nargin<7
    dy=0.001;
end
if nargin<8
    I4=0;
end
y=0:dy:1;
Omega=sqrt(alpha*(1i*omega+omega.^2));

% start calculations
psi=cosh((y-1)/(lambdaBar))/cosh(1/lambdaBar);
% psi=exp(-y/lambdaBar);
I1=zeros(size(omega));
I2=zeros(size(omega));
I3=zeros(size(omega));
C1=(1-1i*omega)./(Omega.^2);
C2=(1-1i*omega)./(1+Omega.^2*(lambdaBar)^2);
cosOmega=cos(Omega);
parfor i=1:length(y)
    dI1=C1.*(1-(cos(Omega*(1-y(i))))./cosOmega)*psi(i);
    I1=I1+dI1*dy;
    dI2=C2.*(psi(i)-(cos(Omega*(y(i)-1)))./cosOmega)*psi(i);
    I2=I2+dI2*dy;
    dI3=cosh(zeta*psi(i));
    I3=I3+dI3*dy;
end
EsBar=-I1./(I2+J.*(I3+Du+I4));

Qpdf=zeros(size(omega));
Qeof=zeros(size(omega));
for i=1:length(y)
    Updf=C1.*(1-(cos(Omega*(1-y(i))))./cosOmega);
    Ueof=EsBar.*C2.*(psi(i)-(cos(Omega*(y(i)-1)))./cosOmega);
    Qpdf=Qpdf+abs(Updf)*dy;
    Qeof=Qeof+abs(Ueof)*dy;
end
Q=(Qpdf+Qeof);
end
```

D.4 Simplified Bandopadhyay model with absolute flow

```
function [I1,I2,I3,E,Q,Omega]= BandopadhyayModelFreqSimpleAbs(omega,alpha,lambdaBar,J,Du,I4
    )
narginchk(4,6)
if nargin==4
    Du=0;
end
if nargin==5
    I4=0;
end
Omega=sqrt(alpha*(1i*omega+omega.^2));
I1=lambdaBar*(1-1i*omega).*(lambdaBar^2-lambdaBar.*tanc(Omega));
I2=-lambdaBar*(1-1i*omega).*(1/2+lambdaBar*Omega.*tan(Omega));
I3=1*ones(size(omega));
E=-I1./(I2+J.*(I3+Du+I4));
Q=abs((1-1i*omega)./Omega.^2.*(1-tanc(Omega)))...
    +abs(E.*(1-1i*omega).*(lambdaBar-tanc(Omega)));
end
```

D.5 Bandopadhyay model with an load resistance

```
function [i1,i2,i3,EsBar,Q,psi]=BandopadhyayModelFreqLoad(omega,alpha,lambdaBar,zeta,J,Du,
    i4,dy)
% omega=omega*
% omega_=omegaBar
y=0:dy:1;
omega_=1i*omega+omega.^2;

% start calculations
psi=cosh((y-1)/(lambdaBar))/cosh(1/lambdaBar);

i1=zeros(size(omega));
i2=zeros(size(omega));
i3=zeros(size(omega));
C1=(1-1i*omega)./(alpha*omega_);
C2=(1-1i*omega)./(1+alpha*omega_*(lambdaBar)^2);
sqrtAlphaOmega_=sqrt(alpha*omega_);
cosSqrtAlphaOmega_=cos(sqrtAlphaOmega_);
parfor i=1:length(y)
    dI1=C1.*(1-(cos(sqrtAlphaOmega_*(1-y(i))))./cosSqrtAlphaOmega_)*psi(i);
    i1=i1+dI1*dy;
    dI2=C2.*(psi(i)-(cos(sqrtAlphaOmega_*(y(i)-1)))./cosSqrtAlphaOmega_)*psi(i);
    i2=i2+dI2*dy;
    dI3=cosh(zeta*psi(i));
    i3=i3+dI3*dy;
end
EsBar=-i1./(i2+J*(i3+Du+i4));

Q=zeros(size(omega));
parfor i=1:length(y)
    dQ=C1.*(1-(cos(sqrtAlphaOmega_*(1-y(i))))./cosSqrtAlphaOmega_)+...
        EsBar.*C2.*(psi(i)-(cos(sqrtAlphaOmega_*(y(i)-1)))./cosSqrtAlphaOmega_);
    Q=Q+dQ*dy;
end
end
```

D.6 Flow profile using the Bandopadhyay model

```
function [I1,I2,I3,EsBar,Updf,Ueof,psi]=BandopadhyayModelFlow(omega,alpha,lambdaBar,zeta,J
    ,Du,dy)
y=0:dy:1;
%omega = omegaStar;
omega_=1i*omega+omega.^2;%omega bar

% start calculations
psi=cosh((y-1)/(lambdaBar))/cosh(1/lambdaBar);

I1=zeros(size(omega));
I2=zeros(size(omega));
I3=zeros(size(omega));
C1=(1-1i*omega)./(alpha*omega_);
C2=(1-1i*omega)./(1+alpha*omega_*(lambdaBar)^2);
sqrtAlphaOmega_=sqrt(alpha*omega_);
cosSqrtAlphaOmega_=cos(sqrtAlphaOmega_);
for i=1:length(y)
    dI1=C1.*(1-(cos(sqrtAlphaOmega_*(1-y(i)))./cosSqrtAlphaOmega_)*psi(i);
    I1=I1+dI1*dy;
    dI2=C2.*(psi(i)-(cos(sqrtAlphaOmega_*(y(i)-1)))./cosSqrtAlphaOmega_)*psi(i);
    I2=I2+dI2*dy;
    dI3=cosh(zeta*psi(i));
    I3=I3+dI3*dy;
end
EsBar=-I1./(I2+J*(I3+Du));

Updf=zeros(length(omega),length(y));
Ueof=Updf;
for i=1:length(omega)
    Updf(i,:)=C1(i)*(1-cos(sqrtAlphaOmega_(i)*(1-y))/cosSqrtAlphaOmega_(i));
    Ueof(i,:)=EsBar(i)*C2(i)*(psi-cos(sqrtAlphaOmega_(i)*(y-1))/cosSqrtAlphaOmega_(i));
end
end
```

D.7 Flow profile using the simplified Bandopadhyay model

```
function [I1,I2,I3,EsBar,Updf,Ueof,psi]=BandopadhyayModelSimpleFlow(omega,alpha,lambdaBar,
    J,Du,dy)
y=0:dy:1;
%omega = omegaStar;
omegaBar=1i*omega+omega^2;%omega bar
Omega=sqrt(alpha*omegaBar);
% start calculations
%psi=cosh((y-1)/(lambdaBar))/cosh(1/lambdaBar);
psi=exp(-y/lambdaBar);


I1=zeros(size(omega));
I2=zeros(size(omega));
I3=zeros(size(omega));
C1=(1-1i*omega)/(Omega^2);
C2=(1-1i*omega)/(1+(Omega*lambdaBar)^2);
cosOmega=cos(Omega);
I1=sum(C1*(1-(cos(Omega*(1-y)))/cosOmega).*psi)*dy;
I2=sum(C2*(psi-(cos(Omega*(y-1)))/cosOmega).*psi*dy);
I3=1;
EsBar=-I1./(I2+J*(I3+Du));

Updf=C1*(1-cos(Omega*(1-y))/cosOmega);
Ueof=EsBar*C2*(psi-cos(Omega*(y-1))/cosOmega);
end
```